10-30-2020

Empirical Investigation of Flow Reversal Strategy in Aftertreatment System

Li Liang
University of Windsor

EMPIRICAL INVESTIGATION OF FLOW REVERSAL STRATEGY IN AFTERTREATMENT SYSTEM

by

Li Liang

A Thesis
Submitted to the Faculty of Graduate Studies
through the Department of Mechanical, Automotive, and Materials Engineering
in Partial Fulfillment of the Requirements for
the Degree of Master of Applied Science at the
University of Windsor

Windsor, Ontario, Canada

2020

Empirical Investigation of Flow Reversal Strategy in Aftertreatment System

by

Li Liang

APPROVED BY:

_____

X. Nie
Department of Mechanical, Automotive and Materials Engineering

_____

J. Tjong
Department of Mechanical, Automotive and Materials Engineering

_____

G. Reader, Co-Advisor
Department of Mechanical, Automotive and Materials Engineering

_____

M. Zheng, Co-Advisor
Department of Mechanical, Automotive and Materials Engineering

September 08, 2020

DECLARATION OF ORIGINALITY

I hereby certify that I am the sole author of this thesis and that no part of this thesis has been published or submitted for publication.

I certify that, to the best of my knowledge, my thesis does not infringe upon anyone's copyright nor violate any proprietary rights and that any ideas, techniques, quotations, or any other material from the work of other people included in my thesis, published or otherwise, are fully acknowledged in accordance with the standard referencing practices. Furthermore, to the extent that I have included copyrighted material that surpasses the bounds of fair dealing within the meaning of the Canada Copyright Act, I certify that I have obtained a written permission from the copyright owner(s) to include such material(s) in my thesis and have included copies of such copyright clearances to my appendix.

I declare that this is a true copy of my thesis, including any final revisions, as approved by my thesis committee and the Graduate Studies office, and that this thesis has not been submitted for a higher degree to any other University or Institution.

ABSTRACT

The flow reversal strategy is categorized as one type of the active flow control strategies. Previous research results have shown that the reaction heat of the catalysts in the aftertreatment system can be trapped by the flow reversal strategy, which is beneficial for the enhancement of the conversion efficiency of the aftertreatment system. In order to better understand the operational principle of the flow reversal system, an active flow aftertreatment system that employs flow reversal strategy has been developed in the Clean Combustion Engine Lab at the University of Windsor.

The main objective of this study is to investigate the heat retention ability of the flow reversal system. In order to make the flow reversal unit work efficiently, the appropriate operational parameters are identified first under a constant inlet gas temperature condition. A comparative study is then conducted to investigate the heat retention capability of both unidirectional and reversal flow during a DOC catalyst cooling down process. Additionally, this thesis also compiles detailed documentation of the flow reversal platform setup and its working principle, which is a valuable research tool to conduct more studies on the active flow control strategies in aftertreatment.

DEDICATION

This thesis is dedicated to my loving family:

My parents Fengmei Zheng, Xiuling Liang

My wife Hua Zhu, and my daughter Kexin Liang

My sister Miya Liang

ACKNOWLEDGEMENTS

I am sincerely grateful to my supervisors, Dr. Ming Zheng and Dr. Graham T. Reader for their support, encouragement, and guidance throughout my Master's degree studies at the University of Windsor. Their wisdom and enthusiasms for research have inspired me to face every challenge encountered throughout the development of this thesis.

I would like to thank the thesis committee members, Dr. Jimi Tjong, Dr. Xueyuan Nie for their precious time, giving me constructive criticism and guidance of my thesis.

I would like to express my thanks to all my dear colleagues and team members at the Clean Combustion Engine Laboratory, Dr. Meiping Wang, Dr. Shui Yu, Dr. Xiao Yu, Dr. Qingyuan Tan, Zhenyi Yang, Hua Zhu, Simon Leblanc, Navjot Sandhu, Linyan Wang, Divyanshu Purohit. Your enormous support is greatly appreciated. I would like to thank Dr. Xiao Yu for his invaluable advice. I also want to thank Navjot Sandhu and Cavan Matthew Hesketh for their assistances with the installation of the flow reversal system, and their help with the experiments.

I would like to give my thanks for all the technical support I received from our faculty members, Kevin Harkai, Bruce Durfy, and Dean Poublon during the setup of the research platform.

Finally, I would like to thank my family – my parents, my wife and my daughter for their love and support.

TABLE OF CONTENTS

LIST OF TABLES

LIST OF FIGURES

LIST OF ABBREVIATIONS/SYMBOLS

BEVs	Battery Electric Vehicles
BTE	Brake Thermal Efficiency
CCEL	Clean Combustion Engine Lab
CDPF	Catalytic Diesel Particulate Filter
CI	Compression Ignition
CPSI	Cells Per Square Inch
DOC	Diesel Oxydation Catalyst
DPF	Diesel Particulate Filter
DME	Dimethyl Ether
EGR	Exhaust Gas Recirculation
EPA	Environmental Protection Agency
FCEVs	Fuel Cell Electric Vehicles
FPGA	Field Programmable Gate Array
FR	Flow Reversal
FRO	Flow Reversal Operation
FTIR	Fourier Transform Infrared Spectroscopy
HC	Hydrocarbon
HCCI	Homogenous Charge Compression Ignition
HCLD	Heated Chemiluminescence Detector
HEVs	Hybrid Electric Vehicles
HFID	Heated Flame Ionization Detector
ICE	Internal Combustion Engine
ICEV	Internal Combustion Engine Vehicle
LNT	Lean NO_X Trap
LTC	Low Temperature Combustion
MAF	Mass Air Flow
NDIR	Non-dispersive Infrared Detector
NI	National Instruments
PM	Particulate Matter

SCR	Selective Catalytic Reduction
SI	Spark Ignition
THC	Total Hydrocarbons
TWC	Three-way Catalyst
UHCs	Unburnt Hydrocarbons
λ	Excess Air Ratio

CHAPTER 1 INTRODUCTION

1.1 Background

The internal combustion engines (ICE) presently power more than 98% of vehicles on the road, and account for 24% of greenhouse emissions worldwide [1, 2]. Consequently, the reduction of the fuel consumption and exhaust emissions of internal combustion engine vehicles (ICEVs) is becoming vital for engine researchers and automotive manufacturers. Battery electric vehicles (BEVs) are considered to be one of the promising alternatives for ICE vehicles, owing to the relatively high "Tank to wheel" efficiency and zero local emission characteristics during operation [3]. However, the mainstream adoption of electric vehicles is still hindered by some fundamental impediments, including lower energy density of the battery pack, limited driving range, long charging time, high production cost, and increased vehicle weight [3].

The gravimetric and volumetric energy density of various hydrocarbon fuels and battery packs are illustrated in Figure 1.1 and Figure 1.2 respectively [3]. It can be seen that the gravimetric energy density of the battery pack is less than 1 MJ/kg, which is significantly lower than the energy density of hydrocarbon fuels. Gaseous fuels, including hydrogen, methane, propane, and butane, normally have a higher gravimetric energy density, but a lower volumetric energy density than their counterparts of liquid fuels. The low volumetric energy density of the gaseous fuels in automotive applications generally demands large storage space to produce the desired driving range. This leads to higher storage costs and packaging problems. Therefore, liquid fuels are more suitable for automotive applications owing to the high gravimetric and volumetric energy density. Apart from energy density,

the availability of the fossil fuels makes the liquid fuels, like diesel and gasoline, as the primary energy sources used in the automotive sector.

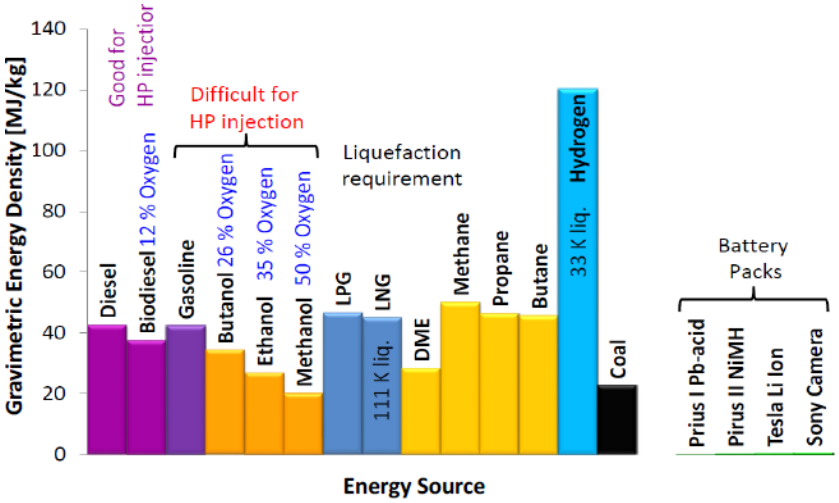

Figure 1.1 Gravimetric energy density of energy sources [3]

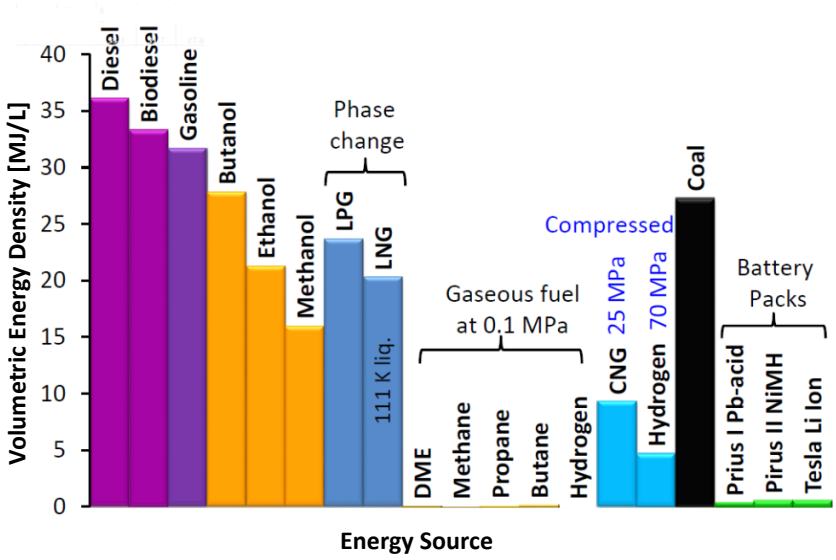

Figure 1.2 Volumetric energy density of energy sources [3]

The lower energy density of battery packs directly affects the driving range and vehicle weight of BEVs. A comparison of the driving range (with a single battery charge/full fuel tank) of BEVs and ICEVs with similar chassis sizes is shown in Figure 1.3 [3]. Passenger cars and light-duty vehicles powered by ICEs can travel over 500 km when carrying 40 kg

hydrocarbon fuels. However, BEVs need to carry a battery pack weighting around 500 kg to have the similar range. Heavy-duty trucks (mostly powered by diesel engines) can travel more than 3000 km when carrying 700 kg of diesel fuel. For the electric trucks travelling the same distance as the diesel heavy-duty trucks, the payload loss is estimated close to 30% [4].

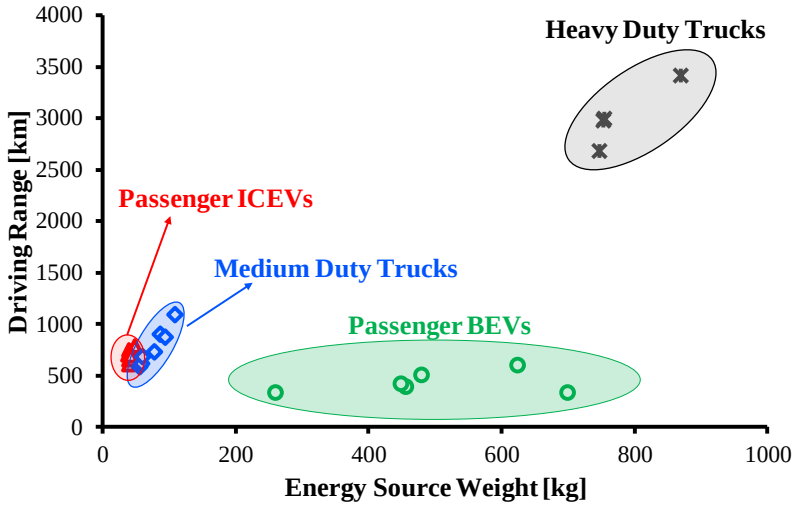

Figure 1.3 Driving range of ICEVs and BEVs [3]

Albeit a steady minor growth can be seen in the global stock of electric passenger cars and light-duty vehicles, the application of electric vehicle still encounters many challenges, namely, limited driving range due to the low energy density, increased vehicle weight by the battery pack, high production cost, and long charging time [3]. The electrification within the heavy and medium-duty vehicle faces even more challenges and practical application issues. Therefore, due to the driving range, load capacity requirements, and the fuel economy considerations, it is projected that the heavy-duty trucks will still be powered by ICEs in the short and long-term globally through 2040 [5].

On the other hand, continuous technological advancements lead to significant efficiency enhancement and emission reduction in ICEs in the past decades, which has also dramatically decreased the impacts on the environment. Considering the impacts on the environment and the energy sustainability and security, future mobility is more likely to be characterized by a mix of solutions, involving BEVs and hybrid electric vehicles (HEVs), fuel cell electric vehicles (FCEVs), and conventional ICEVs. Thus, the internal combustion engine will still play a vital role in the automotive sector [6].

1.2 Challenges for Automotive Internal Combustion Engines

The challenges that are faced by ICEs primarily lie in the efficiency improvement and emission reduction. Combustion in ICEs usually ensues towards the end of the compression stroke. For compression ignition (CI) engines, once the fuel is injected by the fuel-injection system into the engine cylinder, the liquid fuel automizes into small droplets, vaporizing and mixing with the high-temperature, high-pressure air inside the engine cylinder. Once the temperature and pressure in the combustion chamber are above the ignition point of the fuel, spontaneous ignition occurs after a delay period of a few crank angle degrees [7]. Since fuel in CI engines is injected close to the start of combustion, there is almost no knock limit. Therefore, the operation of CI engines allows the use of a higher compression ratio (ranging from 14:1 to 23:1). Owing to the high compression ratio and the overall lean air-fuel mixture, CI engines possess a higher energy efficiency than spark ignition (SI) engines. The brake thermal efficiency (BTE) of CI engines is approximately 40% to 45% [8]. The wide application of the supercharging and/or turbocharging technologies in CI engines also substantially increases their power density, making them more suitable for

heavy-duty applications [9]. Some of the CI engine research platforms have even achieved a BTE of 55% with the acceptable tailpipe emissions [10, 11].

For conventional SI engines, the fuel and air are mixed in stoichiometric ratio at the intake system. The air-fuel mixture is then inducted through the intake valve into the cylinder [12]. Combustion in SI engines is initiated towards the end of the compression stroke at the spark plug gap by an electric discharge. Since the stoichiometric air-fuel mixture is compressed during the compression stroke, knocking and other abnormal combustions, such as pre-ignition and surface-ignition (on hot spark plug electrodes), hinder SI engines to adopt high compression ratios. Because of the stoichiometric combustion and the low compression ratio, SI engines are running at a relatively lower thermal engine efficiency than CI engines. Currently, advancements in SI engines are narrowing the BTE gap between SI engines and CI engines. For instance, Toyota has claimed that the newly developed 2.0-liter hybrid vehicle equipped with an SI engine has achieved a thermal efficiency of 41% [13].

The current trend for modern SI engines is toward engine downsizing and lean/diluted combustion. Turbocharging or supercharging techniques are also applied to compensate for the reduced torque and power performance caused by the downsized engine displacement [12]. The applications of lean mixture or exhaust gas recirculation (EGR) in SI engines dilute the in-cylinder charge. This provides improvements in fuel efficiency and NO_X emission reduction, especially at part load operation [14]. In addition, the adequate air or EGR diluted intake charge potentially allows SI engines to use a higher compression ratio, which further contributes to the improvement of engine efficiency.

The reduction of exhaust emissions during the combustion process is another topic in IC engine research. The exhaust gas in SI engines contains NO_X generated in the high-temperature combustion region, along with carbon monoxide (CO) and unburnt hydrocarbons (UHCs) [12]. For CI engines, the diffusion combustion with overall lean air-fuel mixture inevitably generates high emissions of NO_X, along with soot, CO and HC from the local fuel rich region. The exhaust emissions from IC engines are harmful to the environment and human health, especially NO_X and particulate matter (PM). NO_2 is believed to be the major precursor for smog formation. Regulatory authorities in most governments over the world have introduced increasingly stringent emission norms to control the pollutants from IC engines. The compliance roadmap for heavy-duty CI engines to meet the NO_X and PM emission standards in Environmental Protection Agency (EPA) and the European Union is illustrated in Figure 1.4. The regulations on NO_X and PM have been continuously stringent in the past decades.

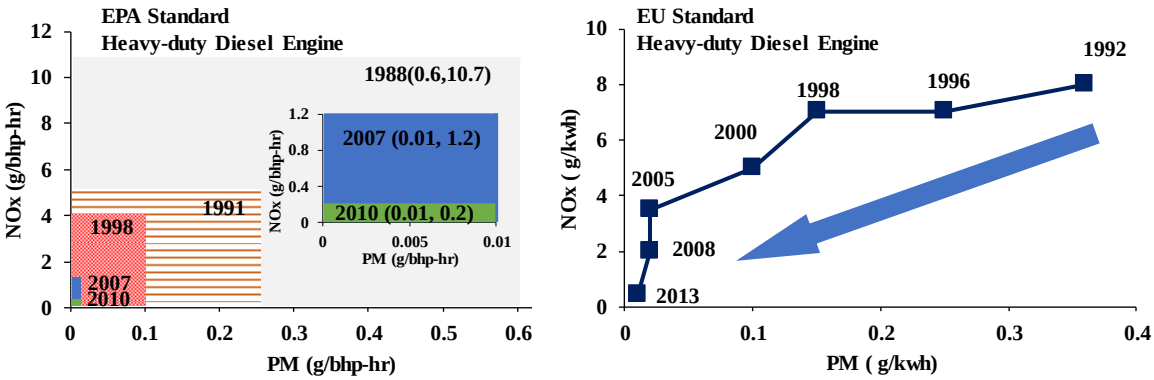

Figure 1.4 Compliance roadmap for NO_X and PM emission

Tremendous efforts have been done to clean up the engine out emissions and improve fuel economy. The applications of some in-cylinder control techniques, such as EGR, low temperature combustion (LTC), etc., are effective in reducing engine out emissions [15].

Moreover, various aftertreatment technologies have also been developed and employed in both CI and SI engines to further reduce the tailpipe emissions [9, 10, 15].

1.3 In-cylinder NO_X-Soot Emission Control

The general goal of in-cylinder NO_X emission control technologies is to reduce the in-cylinder NO_X formation by lowering the flame temperature or reducing the in-cylinder oxygen concentration [15]. These include the application of EGR, the implementation of advanced combustion modes like LTC, and the application of alternative fuels. Each strategy has its benefits and drawbacks [15].

The EGR technology diverts a portion of the exhaust gas back into the intake manifold. It is effective in reducing NO_X formation mainly owing to the dilution, thermal and chemical effects. This is because the exhaust gas primarily consists of N_2, CO_2, and water vapor, with a small amount of O_2. The in-cylinder oxygen can be replaced by N_2, CO_2, and water vapor when the exhaust gas is diverted back to the intake. The presence of CO_2 and water vapor lowers the specific heat capacity ratio of the intake charge, which in turn reduces the flame temperature [15, 16]. However, the reduction of NO_X emission through EGR is usually accompanied by an increase in smoke emission and brake specific fuel consumption, as the lack of oxygen leads to the soot formation on the rich side of the reaction zone, especially under high engine loads [15, 17-18]. This is termed as the classical NO_X-soot trade-off.

LTC is considered to be effective for the simultaneous reductions of NO_X and soot emissions, especially in CI engines. Under LTC mode, the flame temperature is reduced either by operating the engine with a high amount of EGR or operating the engine with a

high excess air ratio (λ) [17]. This can be achieved by heavy EGR or homogeneous charge compression ignition (HCCI) - enabling technologies [19]. However, achieving LTC is challenging, especially in the control of the ignition timing and combustion rate to reduce the cyclic and cylinder-to-cylinder variations. Additionally, a reduced NO_X in LTC mode usually comes with high CO and HC emissions, and combustion noise [20]. To achieve LTC, modern diesel engines are adopted with dual-fuel, multiple-injection, and negative valve overlapping strategies, which are expensive and complicated [17].

Using alternative fuels, including butanol, ethanol, and dimethyl ether (DME), is another way to deal with the NO_X-soot trade-off for CI engines. The combustion of these alternative fuels is nearly soot-free, owing to their fuel-bound oxygen content. At the same time, NO_X can also be reduced through heavy EGR. For instance, the use of n-butanol and diesel in dual fuel CI engines has shown the potential to simultaneously reduce NO_X and soot emissions through the port injection of butanol and direct injection of diesel [21]. Ethanol is also used for port injection, along with diesel direct injection, to achieve HCCI combustion [22]. However, the low NO_X and soot emissions in alternative fuel applications are often achieved at the relatively high total hydrocarbons (THC) and CO emissions [22].

1.4 Aftertreatment Emission Reduction

In addition to the advanced in-cylinder control technologies to reduce the exhaust pollutants from IC engines, many aftertreatment technologies are also well-established and widely used in the automotive industry [23]. The aftertreatment devices in CI engines mainly include diesel oxidation catalyst (DOC), diesel particulate filter (DPF), lean NO_X trap (LNT), and selective catalytic reduction (SCR); or a combination of those [23]. In SI engines, the three-way catalyst (TWC) is widely used to clean up engine out emissions.

1.5 Flow Control Strategies in Aftertreatment System

In an aftertreatment system, the chemical reactions and conversion efficiency of the catalytic converters are highly dependent on the exhaust gas temperature [24]. For example, the required temperature for HC oxidation to reach 80% conversion efficiency is about 400 °C [25]. However, the exhaust gas temperature in CI and SI engines varies in a wide range: from lower than 200 °C under very light loads up to 600 ~ 700 °C under high loads in CI engines [26, 27], and from 300 to 400 °C during idling to 900 °C under high-loads in SI engines [25]. The adoption of the aforementioned advanced in-cylinder combustion technologies will lower down the flame temperature in the combustion chamber, which in turn further reduces the exhaust gas temperature. The conversion efficiency of the aftertreatment system will suffer from the low exhaust gas temperature. Therefore, raising the exhaust gas temperature to an appropriate range is of extreme importance to maintain the working efficiency of the aftertreatment system.

Most ICEs incorporate passive flow aftertreatment systems that involve the passive exhaust gas flow control and the active post fuel injection [28]. A typical passive aftertreatment used in CI engines is illustrated in Figure 1.5 (a) [29]. In order to raise the exhaust gas temperature and reduce NOx emission, the passive aftertreatment system usually requires cyclic fuel rich conditions or post fuel injections in engine operations, which results in extra fuel penalty [29, 30].

Apart from the passive flow aftertreatment system, actively controlling the exhaust gas flow is also helpful to retain and extend the temperature range of the catalysts, thus keeping the catalysts in an appropriate reactive condition with less fuel penalty. This is termed as the active flow aftertreatment control, as shown in Figure 1.5 (b). In the active

aftertreatment system, the air-fuel ratio, the temperature range, and the flow direction of the exhaust gas can be modified through active λ, temperature, and flow controls [27-29, 31].

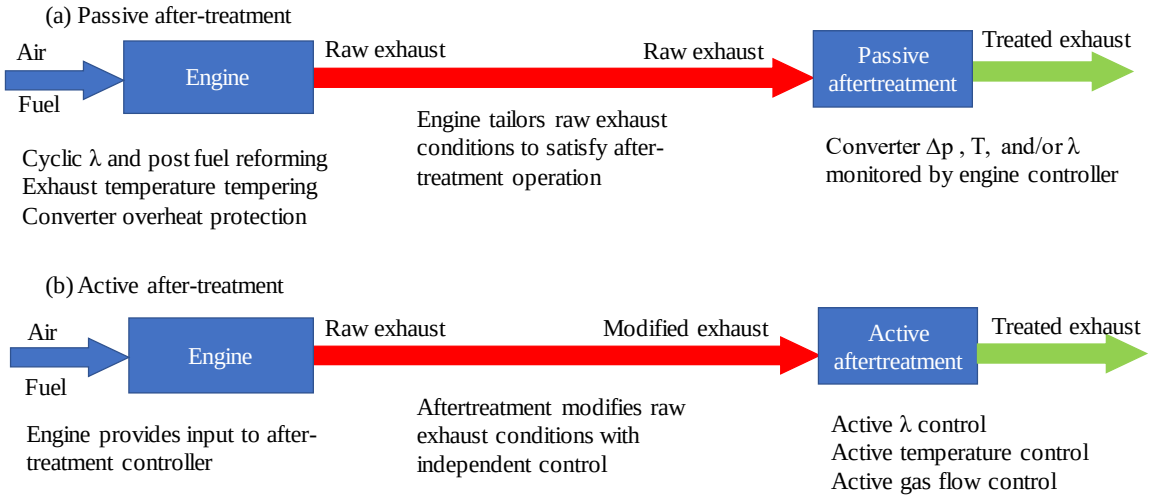

Figure 1.5 Passive versus active aftertreatment system [29]

In terms of the active flow control, four types of strategies have been proposed and widely discussed in the literatures. This includes the parallel alternating flow, partial restricted flow, periodic flow reversal, and extended flow stagnation.

Zheng *et al*. presented the schematics of an alternating parallel flow and a reversal flow in their work and explained the operating principles of these two active flow control strategies, as shown in Figure 1.6 [28]. These two strategies were compared to the conventional passive flow through both simulation and empirical approaches. Relevant results confirmed that the active flow control strategies could effectively maintain the substrate temperature of the catalyst in the target range with supplemental fuels [28].

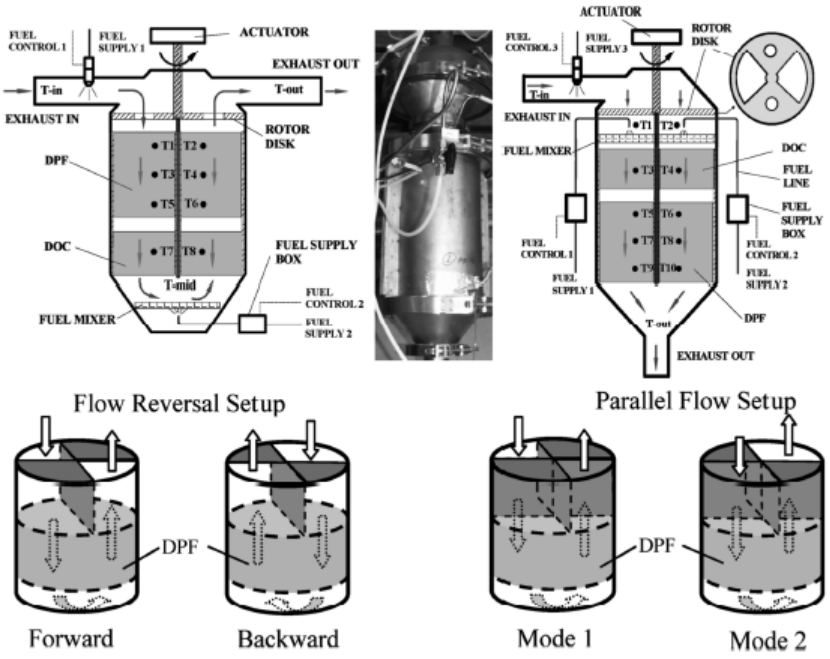

Figure 1.6 Schematic of the active flow control strategies [28]

Schenk *et al*. designed a four-flow-path (parallel-flow) control system equipped with catalytic diesel particulate filter (CDPF) in a heavy-duty diesel engine. The engine results showed a significant reduction in nitrogen oxides (NO_X) and PM by using the parallel-flow control system [32]. A reciprocating-flow regeneration of soot filter was proposed by Konstandopoulos and Kostoglou [33]. They also mathematically modeled the regeneration of the soot filter. The numerical results confirmed that the reciprocating-flow regeneration enhanced the heat recovery in the catalyst, which in turn significantly raised the temperatures of the filter higher than in the conventional regeneration process [33].

Algieri *et al*. compared the energetic performance of the aftertreatment systems with both active and passive flow control strategies [34]. They used a numerical model to simulate the thermal behavior of the aftertreatment system. Through the model, they evaluated the influence of the engine operating conditions on the performance of active and passive flow control systems. They suggested that the active flow control strategy was more suitable to

maintain the substrate temperature of the catalyst for a longer time after sudden changes in the engine load, even under lean and low load conditions. However, the unidirectional flow was preferable when the aftertreatment system encountered with rapid cooling or heating [34, 35].

1.6 Flow Reversal Strategy

The flow reversal (FR) strategy is one of the active flow control strategies. The FR strategy was originally patented by Cottrell in 1983. This strategy was mainly used to enhance the temperature of the catalyst by reversing the direction of the feeding gas.

Liu *et al*. illustrated the early structure and operation principle of the flow reversal converter in a natural gas engine application [36]. In their work, the operation of the flow reversal catalytic converter was controlled through four valves, as shown in Figure 1.7. When the control valves 1 and 4 opened at the same time, the engine exhaust gas flowed into the catalytic converter from left to the right side. This mode was termed as the forward flow, as shown in Figure 1.7 (a). Then valve 2 and valve 3 opened while valve 1 and valve 4 were closing, and the engine exhaust gas flowed into the catalytic converter from right to the left side, as shown in Figure 1.7 (b). This mode was called the reverse flow. The whole cycle consisted of a forward flow and a reverse flow operation [36].

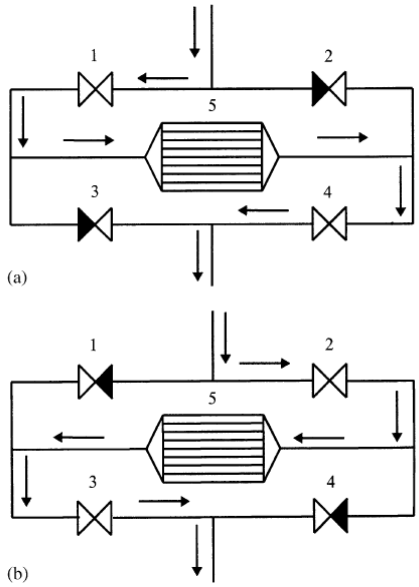

1,2,3,4: control valves 5: catalytic converter

Figure 1.7 Early concept of the reversal flow catalytic converter [36]

Later, Zheng patented a compact reversing flow catalytic converter with the protection from overheating. This design only used one actuator rather than four valves to divert the exhaust gas through the catalytic converter [37]. The catalytic converter had a U-shaped gas pass that communicated with two ports at the top of the canister. A rotor disk that had two openings was mounted on the top of the container, as shown in Figure 1.8 [28, 37, 38]. The actuator could rotate around the perpendicular central axis in three positions. Two positions were corresponding to the forward and backward flow directions respectively. When the catalyst was overheated, the actuator was switched to the third position, so the exhaust gas flow could bypass the catalyst [37].

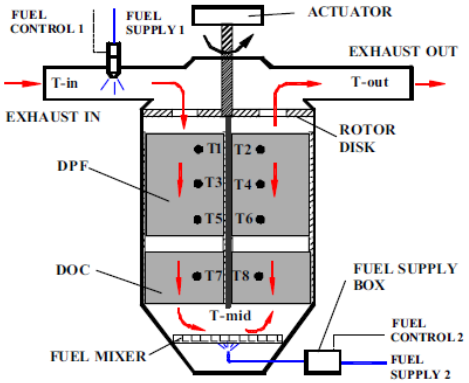

Figure 1.8 Schematic of the compact reversal flow catalytic converter [37, 38]

The essence of the flow reversal strategy is to trap the reaction-generated heat in the catalyst through periodic reversing the flow direction, which in turn accelerates the reaction rate of the catalyst [33]. The basic heat trap effects of the flow reversal strategy are illustrated in Figure 1.9 [36, 39]. Under the forward flow direction, the substrate temperature of the catalyst initially rises slowly as the exothermic reaction starts, and more sharply as the reaction proceeds. The temperature profile of the substrate highly depends on the operating conditions, especially the inlet gas temperature. If the inlet gas temperature is lowered, the exothermic reaction slows down, and the peak temperature of the substrate tends to migrate towards the exit of the reactor, as shown in Figure 1.9 (a) and (b).

When the direction of the feeding gas is switched from the inlet to the exit of the reactor, the energy previously stored in the exit of the reactor is used to heat up the feeding gas. Because this stored energy is added to the feeding gas, it is possible to raise the substrate temperatures of the catalyst higher than the adiabatic temperature rise, based on the temperature of the fresh feeding gas at the inlet [40, 41]. The high temperature region of the substrate moves along with the cool feeding gas, as shown in Figure 1.9 (c) and (d). As periodically reversing the direction of the feeding gas, a quasi-steady-state operation can

be achieved in which the high temperature region stays in the centre of the substrate, as shown in Figure 1.9 (e). The substrate temperature oscillates with the switching of the gas direction.

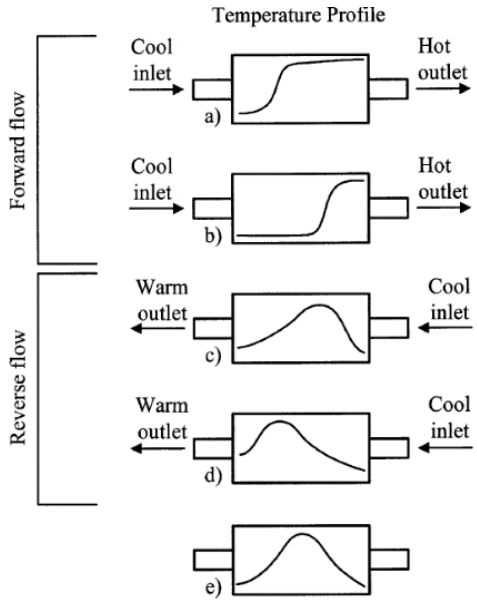

Figure 1.9 Heat trap effect of the flow reversal converter [36]

Previous empirical and simulation efforts were made to explore the heat trap effect of flow reversal strategy on aftertreatment improvement. Matros and Bunimovich reviewed various applications of the flow reversal operation (FRO) under forced unsteady conditions for catalytic reaction [35]. One of the advantages summarized in their work was that the FRO could trap energy within the reactor, which allowed efficient recovery of exothermic reaction heat or substantially reduced energy consumption for endothermic processes [35].

Liu *et al*. investigated the flow reversal catalytic converter in a dual-fuel engine through both experimental and numerical studies [36]. They found that the reversal flow catalytic converter could achieve a high CO and HC conversion efficiency at low inlet temperature under light engine load operation, provided that the initial reactor temperature was sufficiently high [36]. As the reversal flow did not show advantages when the initial reactor

temperature was too low to initiate any reaction, they suggested to preheat the catalyst in the absence of initial high engine load operation for catalyst preheating [36]. Smith studied a reverse-flow oxidation catalyst reactor with supplemental fuel injection in a simulated lean-burn natural gas exhaust mixture [42]. He revealed that the periodical reversing the direction of the exhaust gas flowing through the catalyst trapped the chemical reaction heat. Thus, the overall exhaust gas temperature was raised up. This significantly increased the CH_4 conversion efficiency, otherwise, it was very difficult to oxidize CH_4 under low exhaust gas temperature conditions. For instance, there were 77% of improvement when the reverse-flow operating at 400 °C – 450 °C feeding temperature and 20,000 hr^{-1} space velocities, and 292% improvement at 550 °C – 600 °C feeding temperature and 80,000 hr^{-1} space velocity [42]. Under low engine load conditions, a high methane conversion efficiency could also be achieved through injecting supplemental fuel into the feeding gas [42]. Zheng and Reader studied the flow reversal strategy for lean burn engines [29]. Their results showed that the flow reversal strategy could elevate the temperature in the central region of the oxidation catalyst. The heat generated from high engine load conditions could be retained in the catalyst for a longer time when the engine operation was shifted to low load. Additionally, the flow reversal strategy made the external central heating more effective [29]. However, a low gas mass flow rate with a high HC concentration in the flow reversal strategy had a high tendency to overheat the catalyst [29].

1.7 Objective of Thesis

Previous research results have shown that the flow reversal strategy can retain the reaction heat within the catalyst and improve the conversion efficiency of the aftertreatment system.

In order to better understand the operational principle of the flow reversal system, an active flow control system has been developed in Clean Combustion Engine Lab (CCEL) at the University of Windsor. The main objective of this study is to investigate the heat retention capability of the flow reversal strategy through empirical work. In order to make the flow reversal unit work efficiently, the appropriate operational parameters are identified first. Additionally, a well-established flow reversal system on the aftertreatment test platform is a valuable research tool to conduct further detailed studies on the active flow control strategies in aftertreatment. The setup process of the flow reversal platform is documented diligently in this thesis.

1.8 Thesis Outline

According to the objects of this work, the thesis is organized as follows:

Chapter 1 is an introduction of the research background in this field; Chapter 2 devotes to the experimental setup used for this study; Chapter 3 is a detailed documentation on the design and working principle of the flow reversal system; Chapter 4 is the empirical work conducted on the flow reversal platform to study the heat retain capability of the flow reversal system. Conclusions are included in Chapter 5. During author's MASc study, author's research efforts are also made in the study of lean NOx trap regeneration using dimethyl ether and the preparation of the rapid compression machine platform, as reported in appendix A and appendix B respectively. The outline of the thesis is illustrated in Figure 1.10.

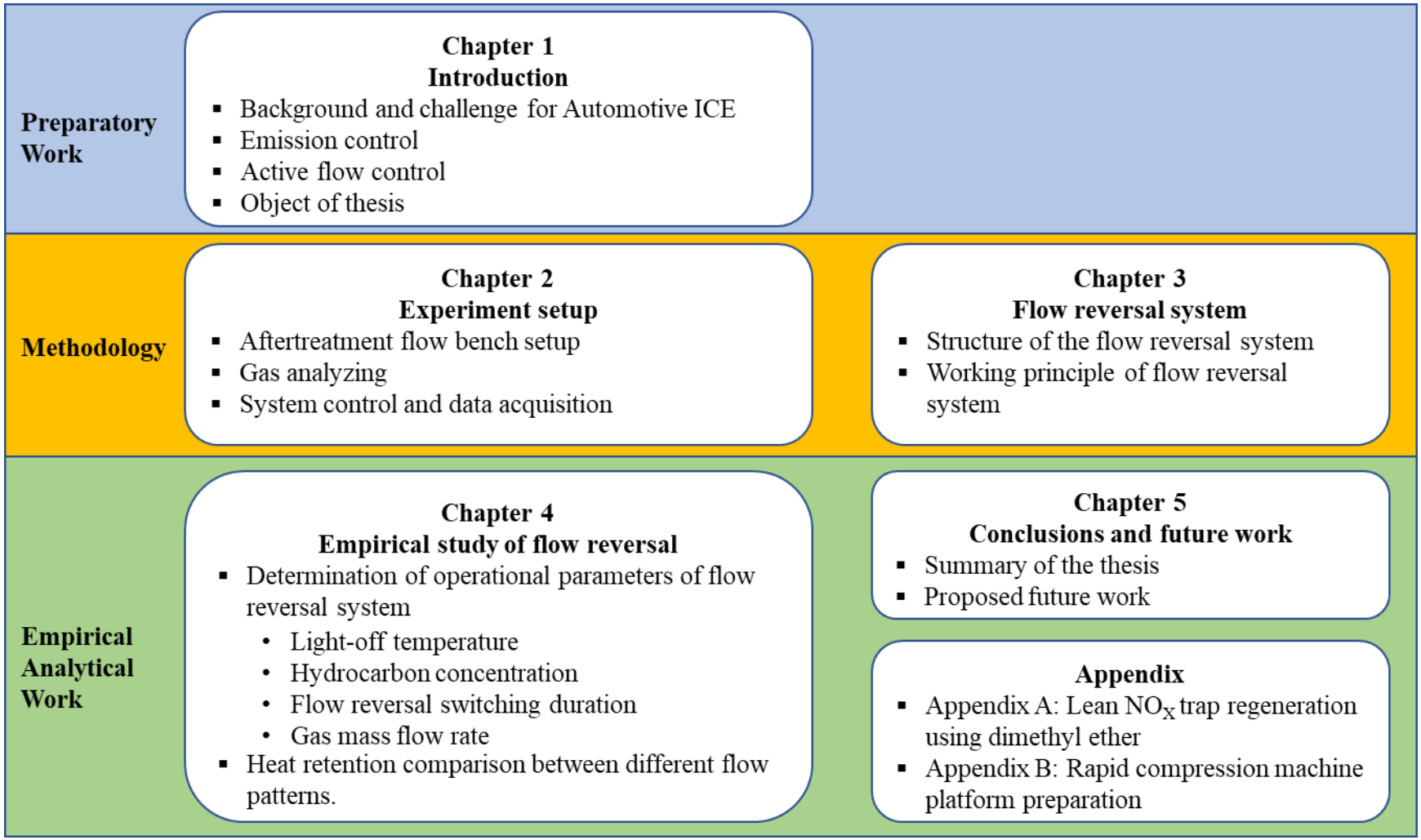

Figure 1.10 Thesis outline

CHAPTER 2 EXPERIMENTAL SETUP

2.1 Aftertreatment Flow Bench

The flow reversal system is installed on an aftertreatment flow bench. The schematic of the experimental setup and the image of the actual flow bench are shown in Figure 2.1 and Figure 2.2 respectively. An Environics Multi-component Gas Mixer is used to control the flow rate of the feeding gas.

During the test, the feeding gas at the inlet of the flow bench is heated up through a Leister 10000S electronic heater with a power of 16 kW. The overall mass flow rate (MAF) is measured through a mass air flow (MAF) sensor (Bosch 0281002619). A port fuel injector is installed at the inlet of the flow reversal canister for fuel injection. In order to reduce the heat loss from the flow bench to the surroundings, all pipes on the flow bench are covered with thermal insulation material.

Two commercially available DOC catalysts are installed inside the canister of the flow reversal system. The cell density of the catalyst is 400 cells per square inch (CPSI). A group of Omega type-K thermocouples with a diameter of 1/16 inches are mounted along the flow bench for temperature measurement. The temperature measurement position includes the upstream and downstream of the flow reversal unit, and the substrate of the DOC catalyst. The response time and the synchronization of the thermocouples are tested offline.

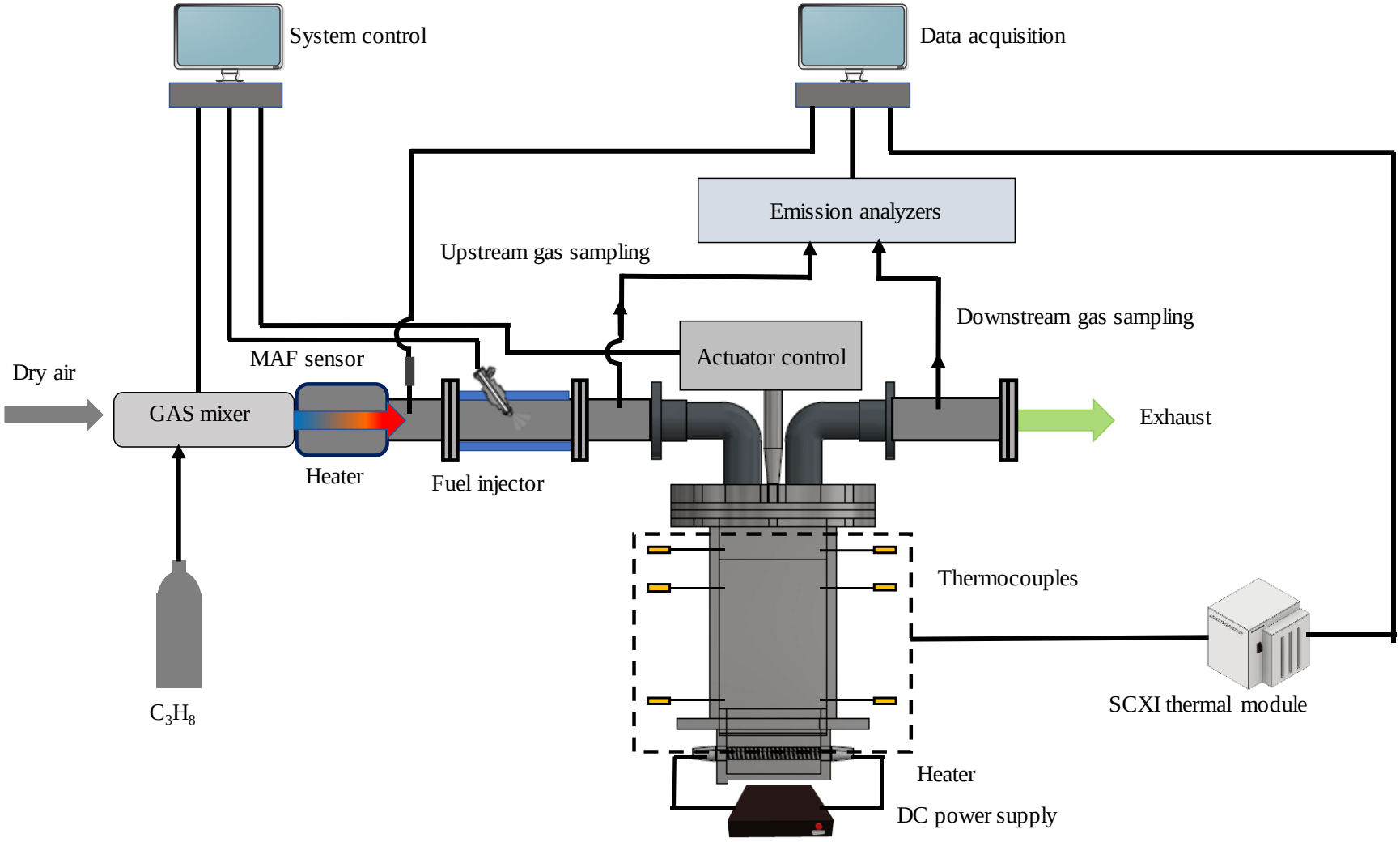

Figure 2.1 Schematic of the flow reversal aftertreatment flow bench setup

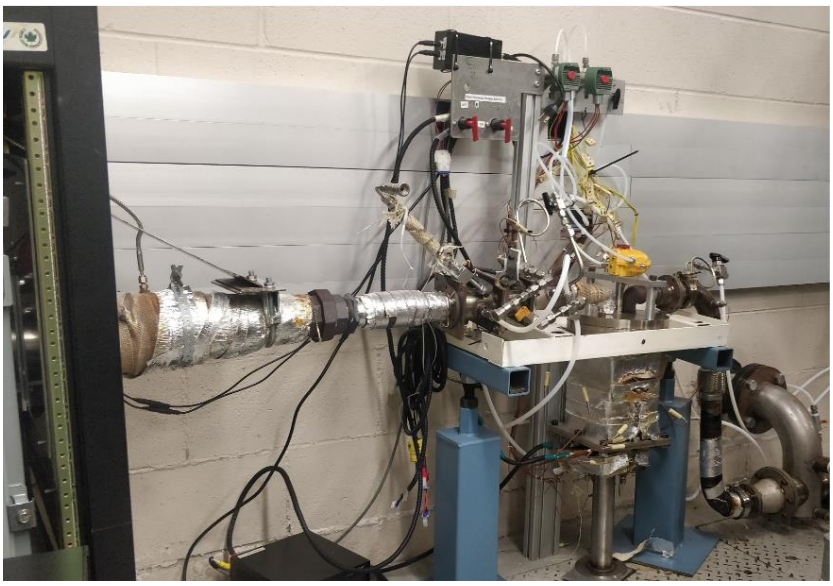

Figure 2.2 Flow reversal aftertreatment flow bench

A heating element with two identical heating wires is installed at the bottom of the flow reversal canister. This heating element is used as an external heating source for the flow reversal unit. It is powered by a constant voltage power supply as shown in Figure 2.3. During this study, the output of the power supply is 180 W. A Tektronix A622 AC/DC probe is used to monitor the current of the heating element, which indicates the working condition of the heating element.

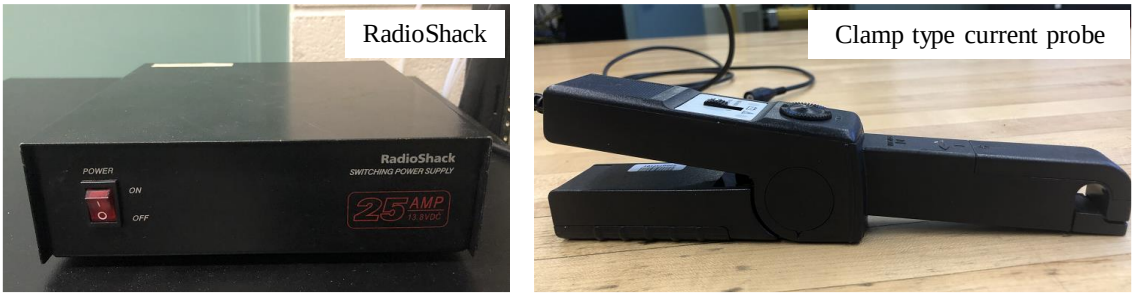

Figure 2.3 Power supply and clamp type current probe

2.2 Gas Analyzers

Gas analyzers are used to measure the concentration and species of the flowing gas at both upstream and downstream of the flow reversal unit. Sampling gases enter a conditioning

unit first to remove the water vapor and particulate matters in the sampling lines. The configurations of the gas analyzers and the conditioning unit are shown in Figure 2.4 and Figure 2.5 respectively.

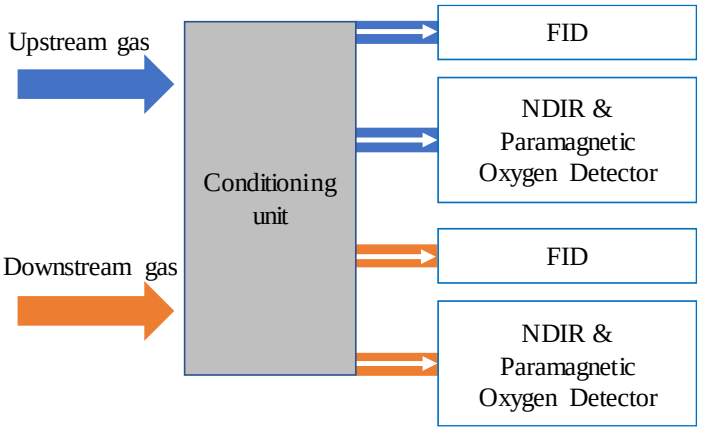

Figure 2.4 Configuration of gas analyzers

Figure 2.5 Conditioning unit for gas analyzers

Non-dispersive Infrared Detector (NDIR) analyzers (CAI 600 series) are used for CO and CO_2 concentration measurements. Paramagnetic Oxygen Detector is used to monitor the O_2 concentration in the flowing gas. Heated Flame Ionization Detector (HFID) analyzer (CAI 300M) is used for hydrocarbon analysis. The specifications and measurement ranges of the gas analyzers are illustrated in Figure 2.6.

CAI 300M-HFID	
➢ Species: Total hydrocarbons ➢ Analysis range: 0-20,000 ppm carbon ➢ Resolution: 0.01 ppm carbon ➢ Gas flow: 3 ± 1.5 L/min ➢ Sample temperature: 0 °C to 50 °C	
CAI- 602P NDIR and oxygen detector	
➢ Species: CO_2, CO, O_2 ➢ Analysis range • O_2: 0-25 % • CO_2: 0-10 % • CO: 0~5000 ppm ➢ Gas flow: 0.5 L/min to 2.0 L/min ➢ Sample temperature: 0 °C to 50 °C	

Figure 2.6 Specifications of gas analyzers

2.3 Control and Data Acquisition System

A National Instruments (NI) SCXI-1303 temperature module installed in an SCXI-1000 chassis is used for temperature acquisition, as shown in Figure 2.7. All the thermocouples are connected to SCXI-1303. The sampling frequency of the temperature measurement in this study is set to 2 Hz.

National Instruments SCXI-1000 Chassis	
System Components ➢ SCXI-1303 temperature module (X3) ➢ SCXI-1302 module 50 pin terminal block (X1) ➢ 32 analog temperature channels per SCXI 1303 module	

Figure 2.7 NI SCXI -1303 temperature acquisition module

The gas concentrations from gas analyzers are also collected instantaneously through a NI data acquisition card. The controlling and data acquisition are integrated into a LabVIEW program with prompt displaying, recording, and parameter setting interface, as shown in Figure 2.8.

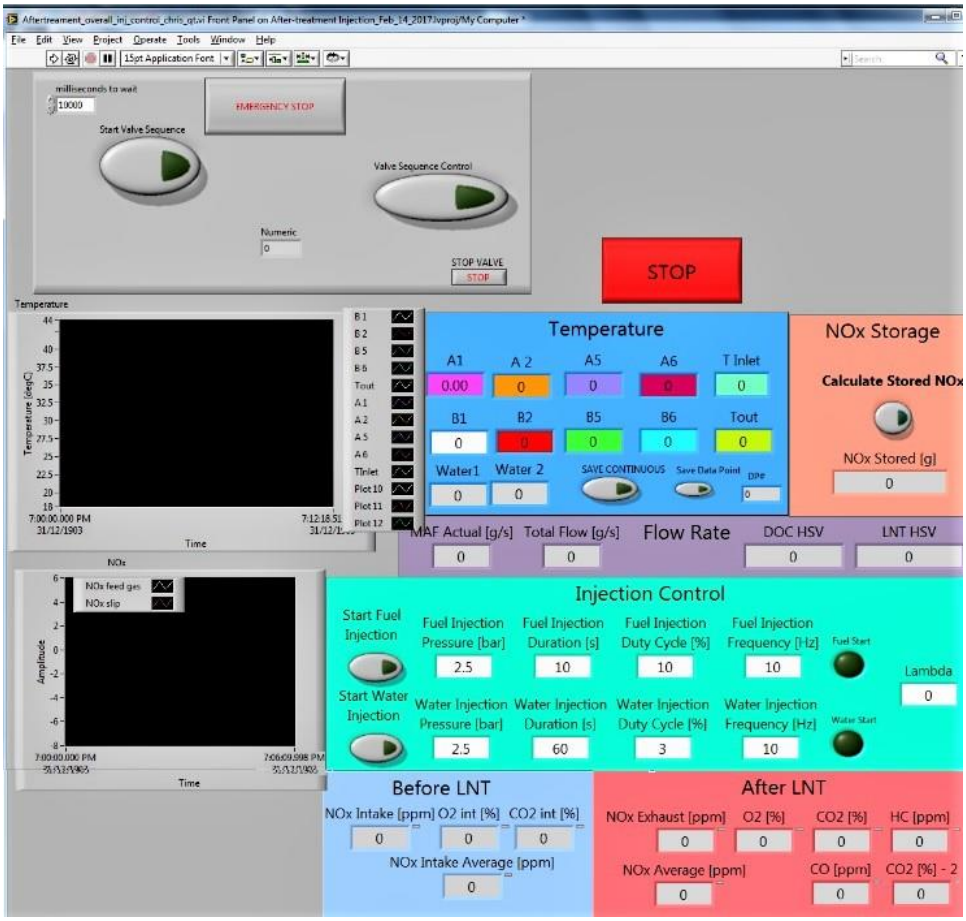

Figure 2.8 LabVIEW program for aftertreatment flow bench

CHAPTER 3 FLOW REVERSAL SYSTEM

The original flow reversal system was designed and fabricated by previous researchers in the author's lab. In this study, a new flow reversal research platform is established based on the previously developed flow reversal unit. The working principle of the current flow reversal system is explained in this chapter. Some challenges experienced during the installation of the flow reversal platform are also documented.

3.1 Structure of the Flow Reversal System

The flow reversal unit used in this study consists of a canister with two compartments, an actuation system, and a rotating valve system. The schematic of the flow reversal unit is shown in Figure 3.1. Detailed descriptions of each part are given in the following subsections.

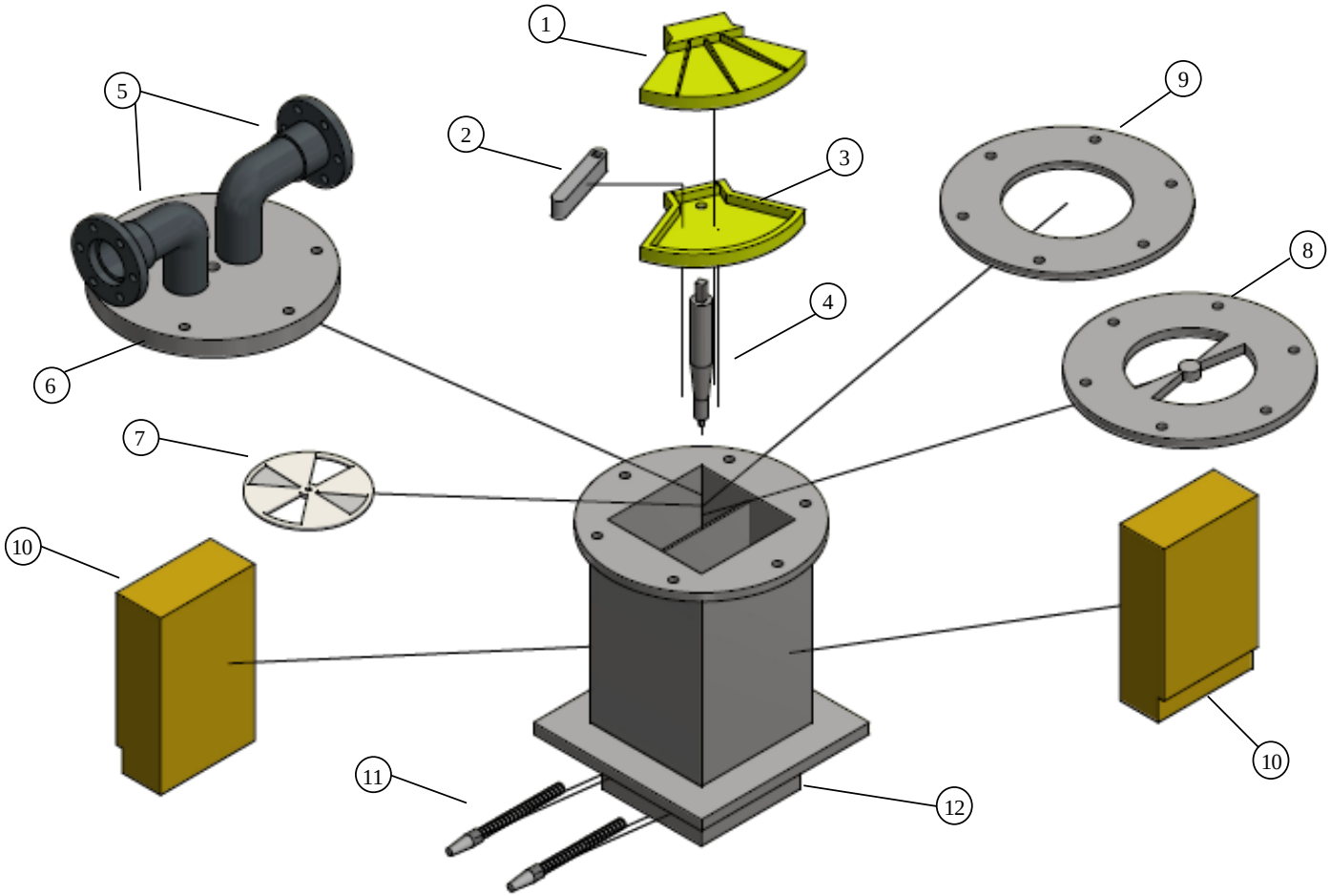

1- Actuator top 2- Actuator vane 3-Actuator bottom 4- Shaft 5- Exhaust pipe (in & out) 6- Top plate 7- Rotor disk 8- Stator 9- Plate bottom 10- DOC catalysts 11- Heating elements 12- Flow reversal main body

Figure 3.1 Schematic of the flow reversal unit

3.1.1 Flow Reversal Canister

The canister in the flow reversal system is in a rectangular shape with a total volume of 2.4 L. The inner space of the canister is separated into two compartments by a metal plate. Two compartments are sharing a common space at the bottom of the canister, as shown in Figure 3.2. Two identical DOC catalysts are placed in each of the compartments. The size of each DOC catalyst is 2 inches by 4 inches by 8 inches. To provide the supplemental energy at the center of the catalyst, a heating element with two identical heating wires connected in series is installed at the bottom of the flow reversal canister.

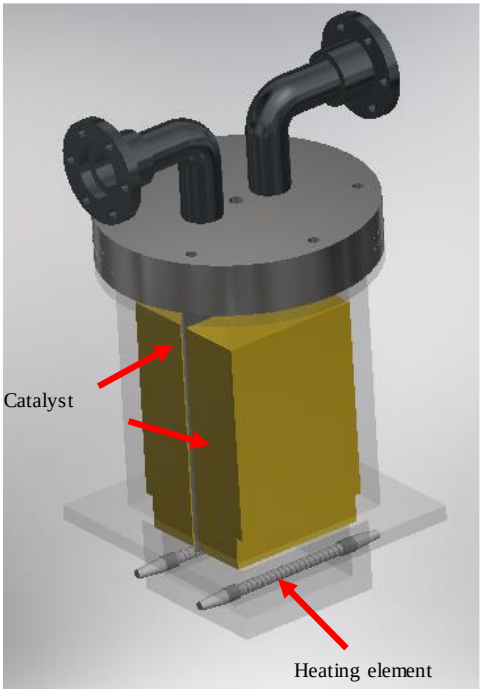

Figure 3.2 Flow reversal canister

3.1.2 Actuation System

An actuation system is used to control the flow direction in the flow reversal unit. It consists of a Kinetrol M03 pneumatic actuator and two three-way solenoid valves. The schematic of the actuator is illustrated in Figure 3.3. The actuator has two compartments with a metal

vane in between. Once a pressure difference is established between the two compartments, the vane inside the actuator is forced to move toward the low-pressure side. The movement of the vane leads to a rotation of the metal shaft that is connected to the rotating valve system. The maximum pressure of the actuator is 7 bar. The operating pressure to drive the actuator in this study is 2 bar absolute.

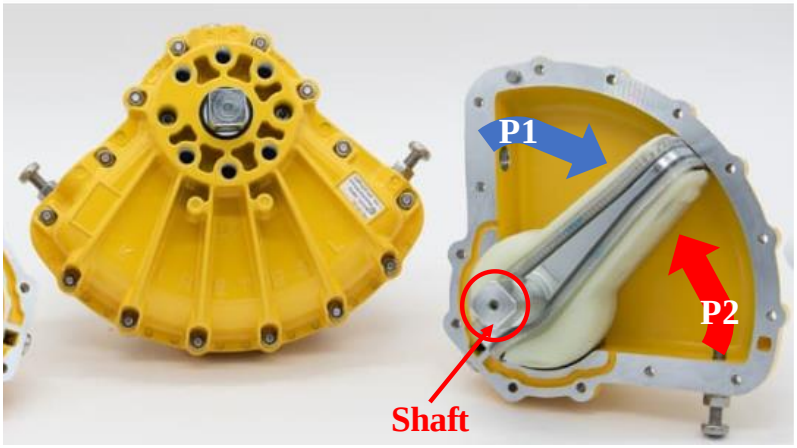

Figure 3.3 Actuator of flow reversal unit

Two three-way solenoid valves are deployed to control the pressure difference between the two compartments of the actuator, which in turn controls the movement of the actuator, as shown in Figure 3.4. As can be seen, one port of the solenoid valve is connected to the driving pressure. Another port is directly exposed to ambient air. The third port of the valve is connected to the actuator. An in-house developed LabVIEW program is used to control the solenoid valve and the working frequency. The control program is illustrated in Figure 3.5.

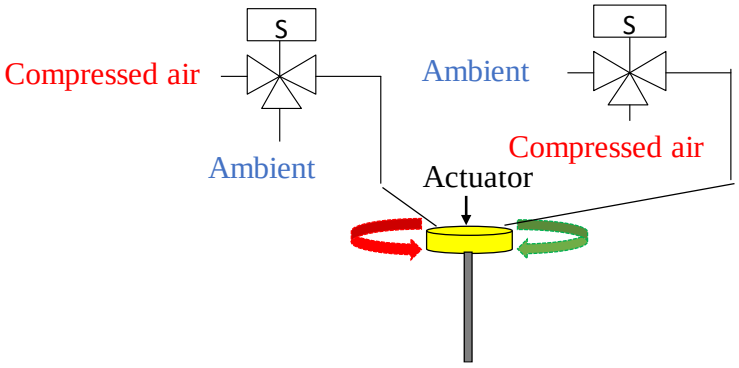

Figure 3.4 Solenoid valve connection

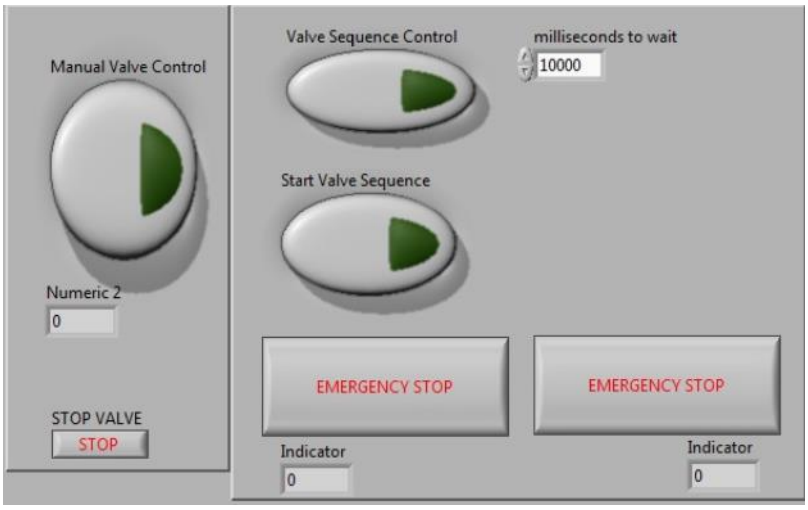

Figure 3.5 Solenoid valve control program

3.1.3 Rotating Valve System

Driven by the actuation system, the rotating valve system in the flow reversal unit is used to guide the actual flow direction through the flow reversal canister. It mainly consists of a rotor disk and a stainless steel shaft. The stainless steel shaft is utilized to connect the actuator and the rotor disk. The shaft converts the movement of the actuator to the rotation of the rotor disk. The shaft is machined into a square shape at both ends, as shown in Figure 3.6.

Figure 3.6 Metal shaft

A specially designed rotor disk is placed on the top of the flow reversal canister. The photo of the rotor disk is shown in Figure 3.7. The rotor disk has two fan-shaped ports that allow the gas to flow through. Driven by the connected metal shaft and actuator, the rotor disk can rotate for a certain angle. This allows the gas to enter the flow reversal canister through one compartment and exit from the other compartment. A pair of compression rings are placed in between the rotor disk and the holding metal plate to seal the gap and reduce gas leakage.

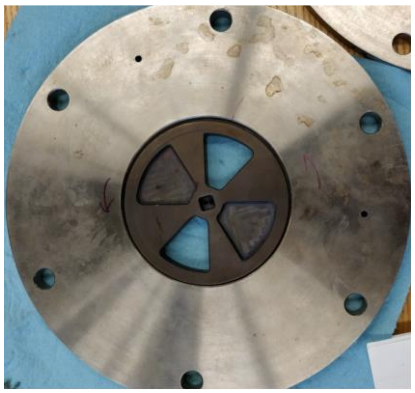

Figure 3.7 Rotor disk of flow reversal unit

The rotation of the rotor disk is driven by the metal shaft. It has been found that the rotor disk tends to expand under high temperature conditions, especially when the flow reversal system has been operated for hours. Once it is expanded, the rotor disk moves increasingly slow and eventually fails to rotate. Abrasion marks have been found on the stator and rotor

disk, as shown in Figure 3.8 (a). To address this issue, a high temperature lubricant is applied between the stator and the rotor, as shown in Figure 3.8 (b). New material with high temperature resistance can be applied for future improvements.

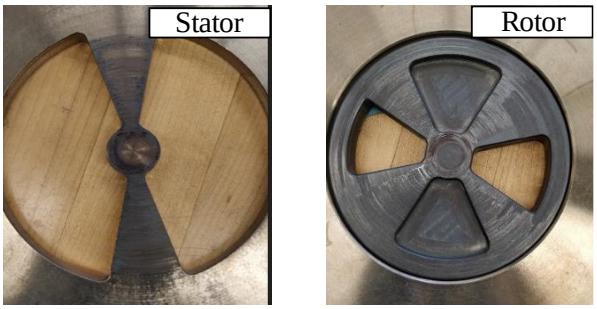

(a) Abrasion marks

(b) High temperature lubricant

Figure 3.8 Applying high temperature lubricant on stator and rotor disk

3.2 Working Principle of Flow Reversal System

The working principle of the current flow reversal unit is illustrated in Figure 3.9. When the rotor disk is in the default position, the flowing gas enters the compartment A of the canister through the hollow fan-shaped port of the rotor disk, and then exits from the compartment B. This is referred to as the forward flow. Once there is a pressure difference generated inside the actuator through the operation of the solenoid valves, the pressure difference drives the vane inside the actuator to move to the low-pressure side. Consequently, the rotor disk rotates with the movement of the actuator. On the rotor disk, the hollow fan-shaped port that allows the flow to enter the compartment A moves to

compartment B. At that moment, the flow direction is changed, and the flowing gas enters the canister through compartment B and exits from compartment A. This is called the backward flow.

One cycle of the flow reversal operation includes both forward flow and backward flow. The duration that each flow direction lasts is controlled through the switching frequency of the solenoid valve.

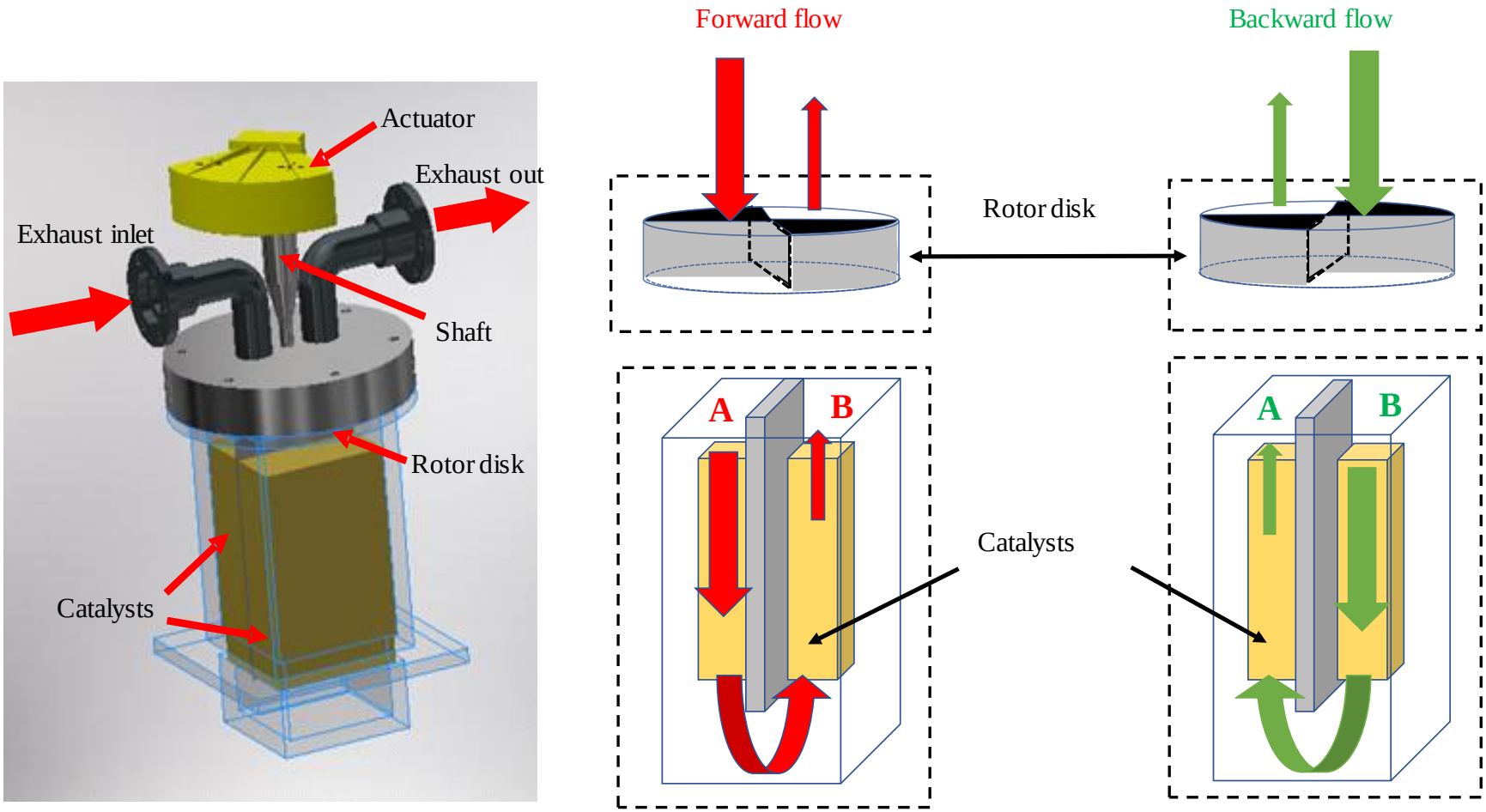

Figure 3.9 Working principle of the flow reversal system

CHAPTER 4 EMPIRCIAL STUDY OF FLOW REVERSAL

The performance of the catalyst in an aftertreatment system is very sensitive to the substrate temperature. Therefore, retaining the heat within the catalyst is crucial for the efficient operation of the aftertreatment system. Since the exhaust gas is one of the major heat sources for the catalyst, the exhaust flow pattern directly affects the substrate temperature. In this chapter, the experimental results conducted on the aftertreatment flow bench are discussed to study the thermal characteristics of the flow reversal system.

Firstly, the effective operational parameters of the flow reversal system were identified under a constant inlet gas temperature condition. These parameters included the flow reversal switching duration, the mass flow rate of the feeding gas, and the hydrocarbon concentration in the feeding gas. The light-off temperature of the DOC catalyst installed in the flow reversal canister was determined using the measured hydrocarbon concentrations at upstream and downstream of the catalyst.

A comparative study of the unidirectional flow and reversal flow was then undertaken through a DOC substrate cooling down process to investigate the heat retention capability of these two flow patterns. The determined light-off temperature was set as the start point of the cooling down process. Propane (C_3H_8) was dosed into the gas flow to simulate the hydrocarbons in the exhaust flow. The hydrocarbon concentrations before and after the DOC during the cooling down process were measured to illustrate the impact of the catalyst temperature on the HC conversion efficiency. The HC concentration was presented in terms of volumetric concentration of C_1 in the gas flow, which corresponded to three times the concentration of the propane dosed in the gas flow.

In order to acquire the temperature profile of the substrate under each test condition, thermocouples were placed at the inlet, front, middle, and rear of the catalyst, as shown in Figure 4.1. For the analysis of the thermal behavior of the catalyst, temperature in the middle of the catalyst was taken as the average of the two middle thermocouples (T_mid 1 and T_mid 2).

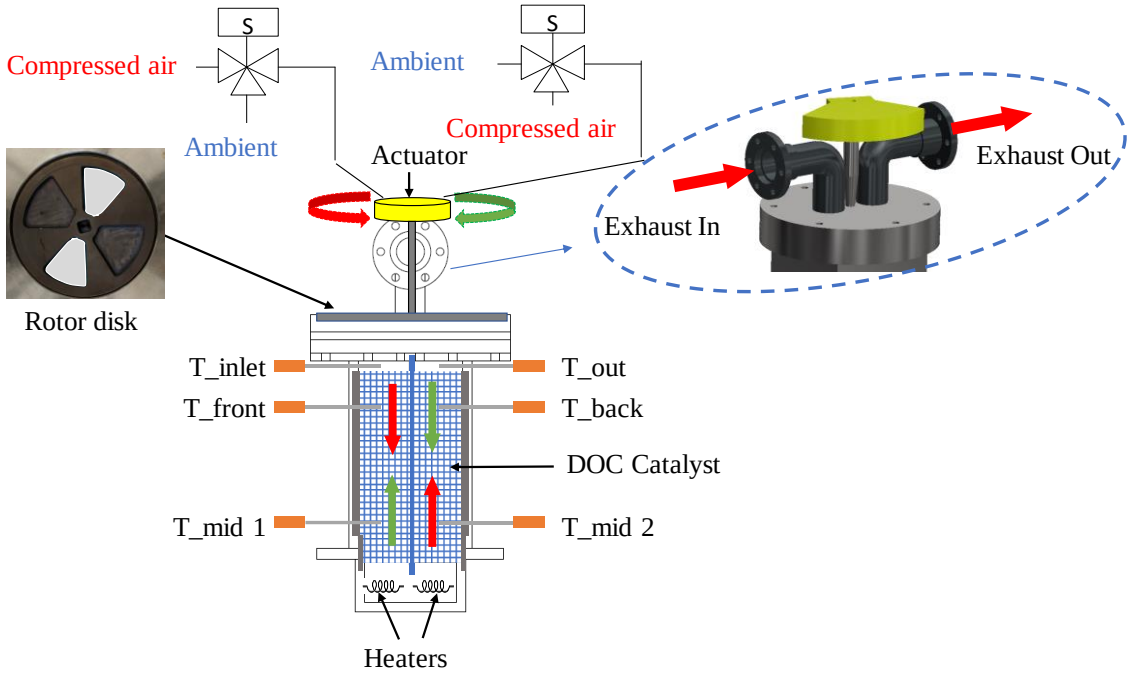

Figure 4.1 Schematic of flow reversal with thermocouple positions

4.1 Determination of Operational Parameters of Flow Reversal System

4.1.1 DOC Light-off Temperature

Catalyst reaches the "light-off" condition when the conversion efficiency of the catalyst reaches 50% [43]. The temperature of the catalyst (denoted by T50) at this condition is defined as the light-off temperature. For oxidation catalyst, the light-off temperature ranges from 350 ℃ to 450 ℃, and is highly dependent on the catalyst type, age, and the HC concentration in the feeding gas [40,41]. To determine the light-off temperature of the DOC

catalyst used in this study, the inlet temperature of the flowing gas was gradually increased from 250 ℃ to 450 ℃. During this process, the HC concentrations before and after the catalyst were measured through the gas analyzers. The HC conversion efficiency was calculated using Equation 1. The HC conversion efficiency of the DOC catalyst under different inlet gas temperatures is illustrated in Figure 4.2. As can be seen, the light-off temperature of the DOC catalyst is about 380 ℃.

$$HC\ conversion\ efficiency = 1 - \frac{HC_{exh}}{HC_{dosing}} \quad (1)$$

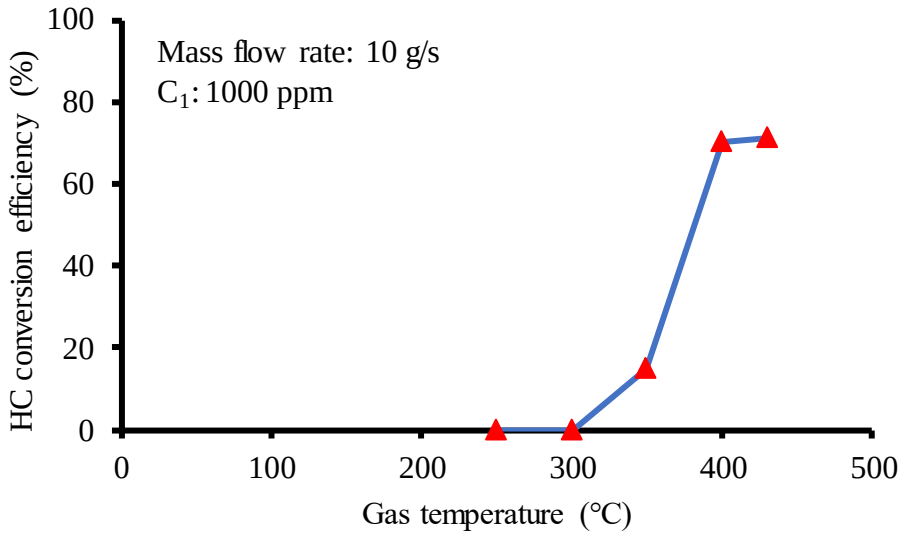

Figure 4.2 HC conversion efficiency under different gas temperatures

For rest of the test, the feed-in gas temperature was set at 430 ℃ which was slightly higher than the light-off temperature of the tested DOC.

4.1.2 HC Concentration

Hydrocarbon concentration is also a factor impacting the substrate temperature after light-off. In order to determine the appropriate hydrocarbon concentration for the studied flow reversal system, C_3H_8 with different concentrations was dosed into the feeding gas. Hereafter, all the hydrocarbon concentrations in this chapter are represented as C_1. During

the test, the feed-in hydrocarbon concentration of C_1 was increased from 1000 ppm to 9000 ppm while the inlet temperature of the feeding gas was maintained at 430 ℃. The corresponding substrate temperatures under different hydrocarbon concentrations were collected and compared. The temperature in the middle of the substrate is shown in Figure 4.3. The results have shown that the average temperature in the middle of the substrate rises with the increase of the concentration of C_1. When 4000 ppm of C_1 was dosed into the gas flow, the temperature in the middle of the substrate reached 470 ℃, which was slightly higher than the inlet gas temperature. Therefore, 4000 ppm of C_1 was selected as the HC concentration for the following cooling down test.

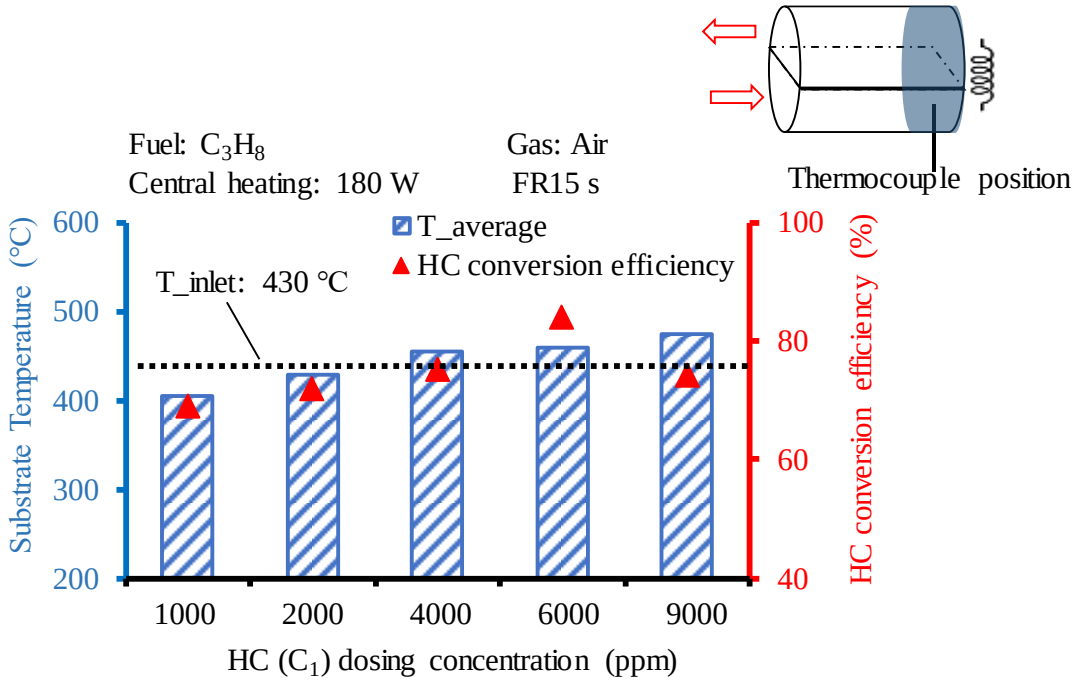

Figure 4.3 Substrate temperature under different HC concentrations

4.1.3 Flow Reversal Switching Duration

The flow reversal switching duration is controlled by the switching frequency between the forward and backward flow. For instance, 10 seconds switching duration means the flow

direction is alternatively changed between forward and backward every 10 seconds, as shown in Figure 4.4.

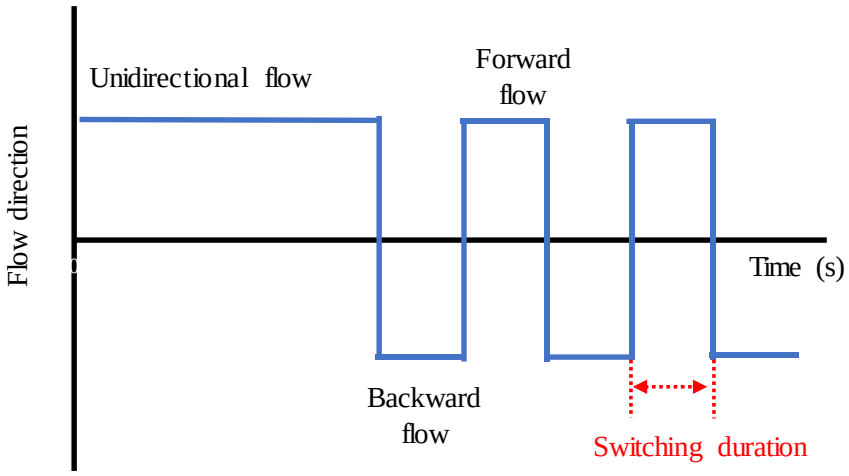

Figure 4.4 Flow reversal switching duration

In order to determine the proper switching duration of the flow reversal system, the temperature profile of the substrate was collected under different switching durations (from 5 seconds to 60 seconds). As the DOC catalysts in both compartments of the canister had the similar temperature distributions under reversal flow condition, the substrate temperature in one of the compartments was selected for presentation of results. The gas mass flow rate was 10 g/s. 4000 ppm of C_1 (hydrocarbon) was dosed into the gas flow at the inlet of the flow bench.

The temperatures in the middle of the substrate under different switching durations are illustrated in Figure 4.5. It can be seen that under 10 g/s mass flow rate, 30 seconds and 60 seconds switching durations lead to more fluctuations in the substrate temperature than the switching duration of 5 seconds and 15 seconds. However, on the other extreme, when switching the flow direction too frequently, every 5 seconds for example, there is

insufficient time for heat to be exchanged between the gas flow and the substrate. Hence, the desired temperature cannot be attained by substrate.

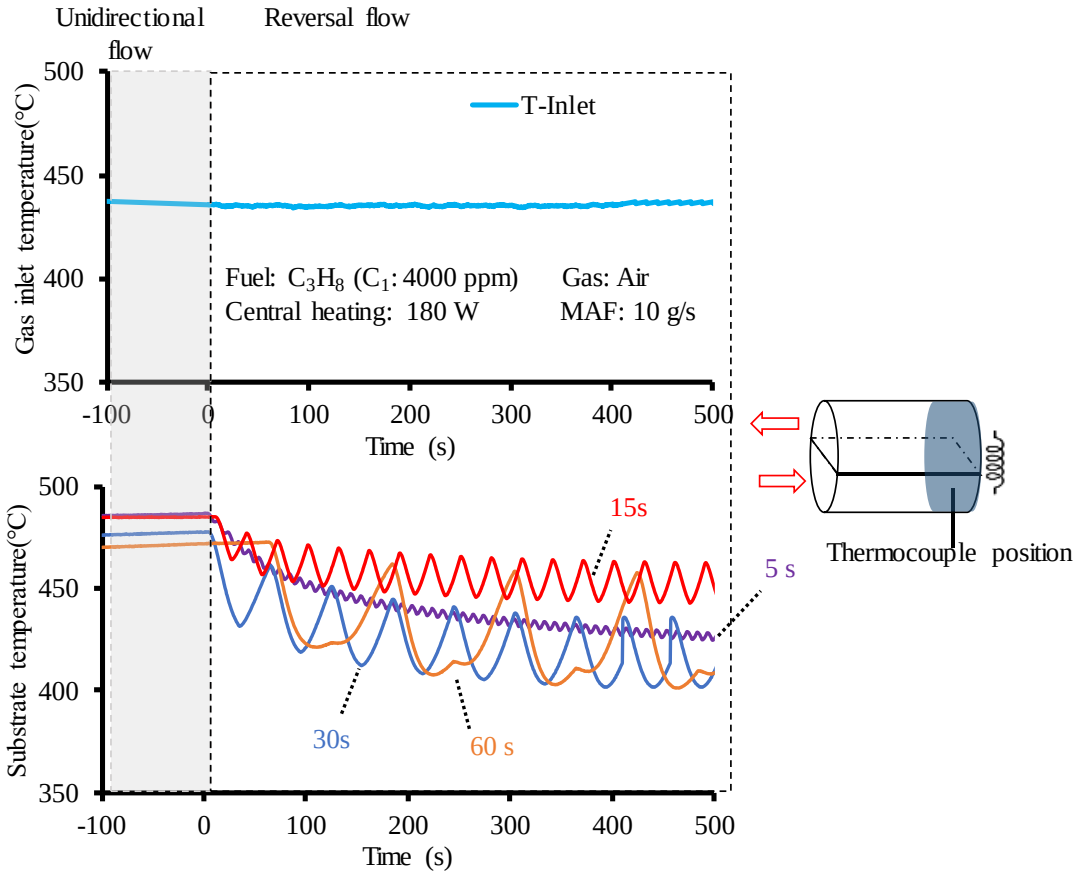

Figure 4.5 Substrate temperature under different switching durations

In addition to the inefficiency of the heat transfer process, it is also not practical to infinitely shorten the switching duration, because the heat retention improvement provided by the flow reversal unit will decline when the solenoid valve and the actuator of the flow reversal system deteriorate due to the excessive wear under high operational frequency [30].

The average temperatures in the middle of the substrate under the corresponding test conditions are shown in Figure 4.6. The switching duration of 15 seconds results in the highest substrate temperature among the other switching durations. Therefore, 15 seconds is the optimum switching duration for the studied flow reversal system.

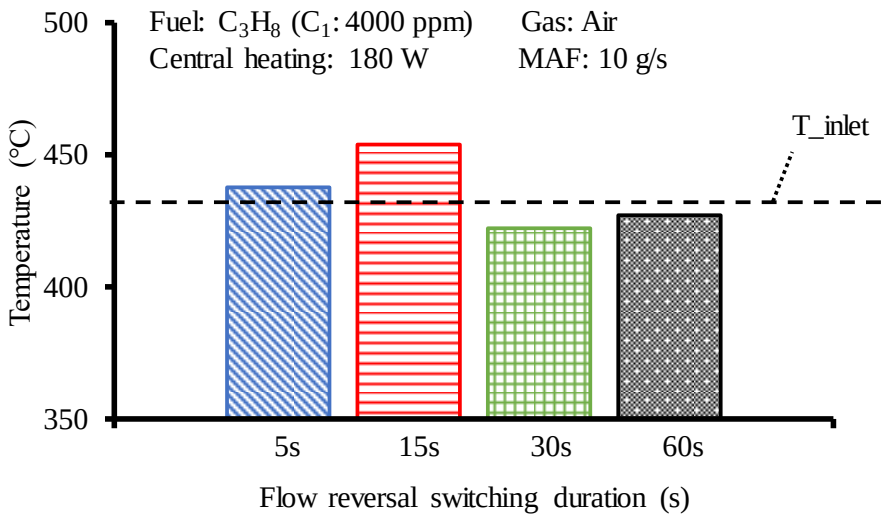

Figure 4.6 Temperature in the middle of the substrate under different switching durations

4.1.4 Gas Mass Flow Rate

The mass flow rate directly affects the heat transfer between the gas flow and the substrate of the catalyst. In order to determine a proper mass flow rate for the studied flow reversal system, 4 g/s, 6 g/s and 10 g/s mass flow rates that were equivalent to the space velocity of 12000 h^{-1}, 18000 h^{-1} and 30000 h^{-1} respectively were selected to investigate the impact of the mass flow rate on the performance of the flow reversal system. It is worth to mention that 10 g/s mass flow rate is the maximum flow rate that the current aftertreatment flow bench setup can reach. During the test, the inlet gas temperature was maintained at 430 °C. 4000 ppm of C_1 was dosed into the gas flow. Because 15 seconds switching duration was determined as one of the optimum switching durations for the studied flow reversal system, the flow reversal switching duration in this set of tests was set to 15 seconds. Under these three mass flow rates, the temperatures in the middle of the substrate were measured and collected, as shown in Figure 4.7.

Under 15 seconds switching duration, the average temperature in the middle of the substrate rises with the increase in the gas mass flow rate. At the mass flow rate of 4 g/s,

the temperature in the middle of the substrate declines rapidly, despite the constant heat addition. However, when the mass flow rate increases to 10 g/s, the substrate temperature is maintained at over 450 ℃ throughout the testing period.

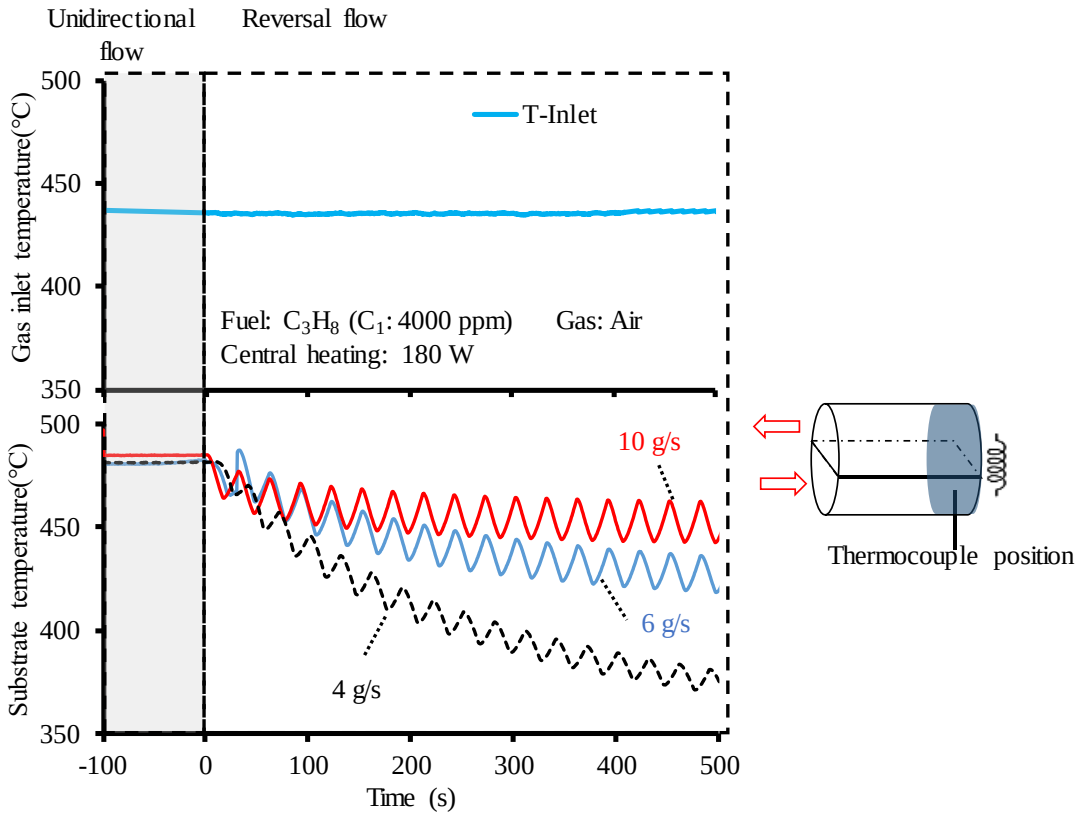

Figure 4.7 Substrate temperature at different mass flow rates

4.2 Heat Retention during Cooling-down Process

4.2.1 Thermal Response during Cooling-down Process

In order to study the heat retention capability of different exhaust gas flow patterns, the DOC catalyst was placed under both unidirectional flow and reversal flow patterns during a cooling down process. Before cooling down, the gas at 430 ℃ under unidirectional flow was fed into the flow bench to heat up the catalyst. 333 ppm of C_3H_8 that was equivalent to 1000 ppm C_1 was dosed into the flowing gas at the inlet of the flow bench. Once the substrate temperature was stable at 430 ℃, the inlet gas temperature was switched to

200 ℃ to cool down the substrate. When relevant tests were conducted under reversal flow condition, the switching duration of the flow reversal system was set to 15 seconds. The experimental parameters are summarized in Table 4-1.

Table 4-1 Test conditions of the cooling down process

Gas temperature (during cooling down)	200 ℃
Hydrocarbon concentration (C_1)	4000 ppm
Mass flow rate	10 g/s
Flow reversal switching duration	15 seconds

The cooling down process is illustrated in Figure 4.8. The gas temperature was switched from 430 ℃ to 200 ℃ once the cooling down process started.

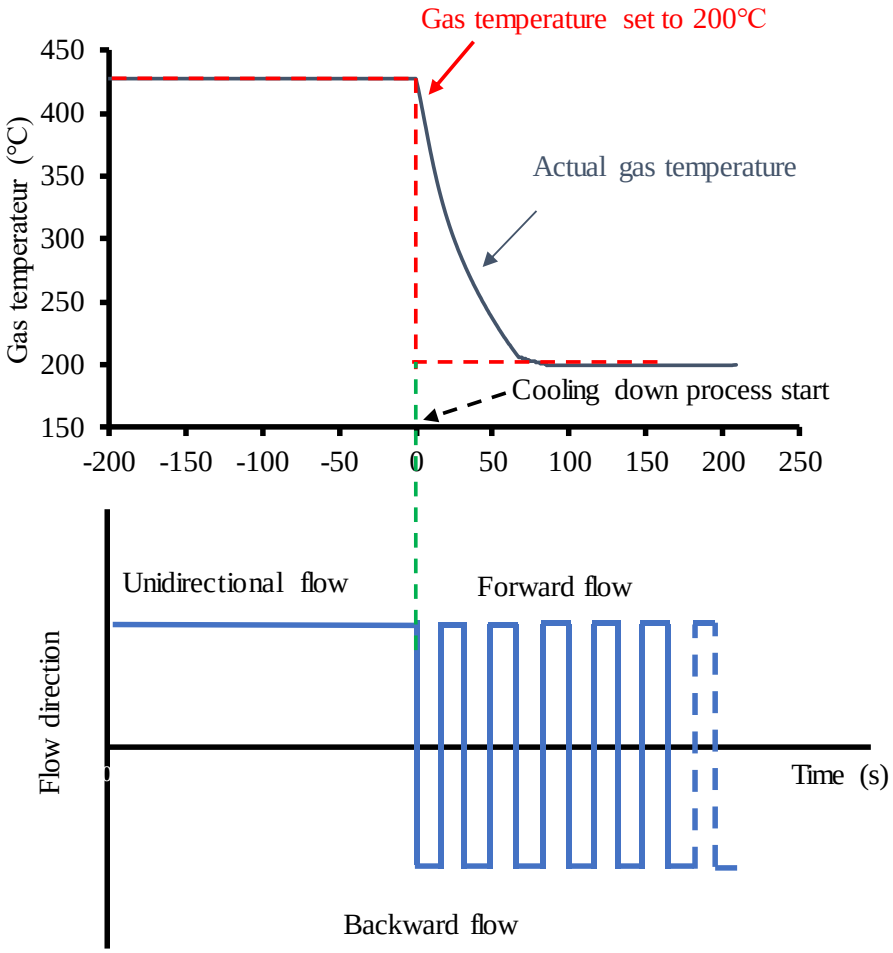

Figure 4.8 DOC cooling down process

The temperatures in the middle of the substrate under both unidirectional flow and flow reversal patterns with 180 W supplemental heating are demonstrated in Figure 4.9. The temperature at the inlet of the canister (T_inlet) represents the gas temperature before the catalyst. Under the unidirectional flow, the substrate is cooled down comparatively fast. The temperature in the middle of the substrate drops 150 ℃ within the first 100 seconds of the cooling down process, as shown in Figure 4.9.

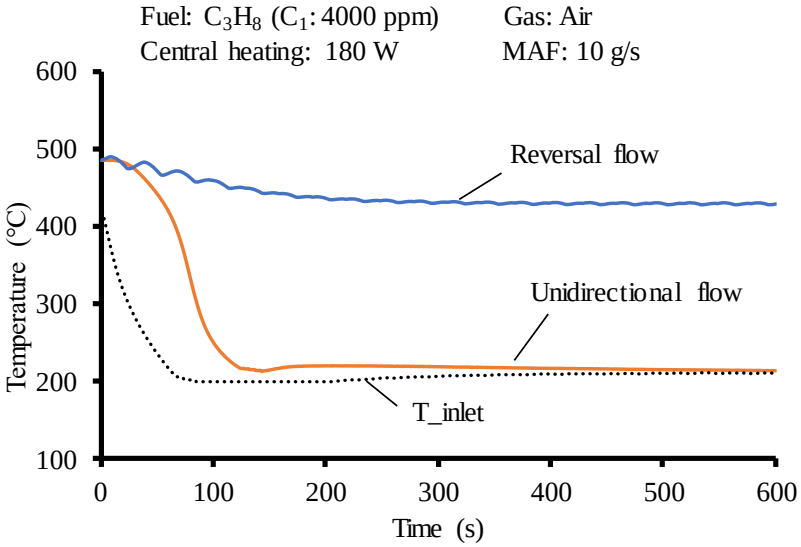

Figure 4.9 Substrate temperature during cooling down process with central heating

In contrast, the substrate is cooled down at a significantly slower rate under the reversal flow scenario. The temperature in the middle of the substrate reduces approximately by 65 ℃ during the test period, as observed in Figure 4.9. This illustrates that the periodic reversal of the gas flow direction can trap the heat within the substrate, which slows down the cooling process.

According to the current literature review, central heating is an effective way for the flow reversal strategy to sustain high temperature from the exothermic reaction inside the DOC. In this study, one heating element with two identical heating wires was installed at the

bottom of the flow reversal canister to supply additional heat to the flow before the latter part of the catalyst. In order to study the impact of central heating on heat retention, cooling down experiments under the same conditions for both unidirectional flow and reversal flow were repeated with supplemental heating.

The temperatures in the middle of the substrate with and without central heating are illustrated in Figure 4.10. Under unidirectional flow, the temperature in the middle of the substrate drops by 150 ℃ within 150 seconds. With 180 W supplemental heating, only 5 ℃ temperature rises (ΔT_{Uni}) can be seen under unidirectional flow at 200 seconds, as compared to the scenario without central heating.

In contrast, under flow reversal strategy, approximately 50 ℃ temperature rises (ΔT_{FR}) can be seen when supplying the same amount of supplemental energy. The substrate temperature is maintained over 450 ℃ during the whole test period with central heating. This indicates that the flow reversal strategy with central heating has a better payoff in temperature rising than the unidirectional flow.

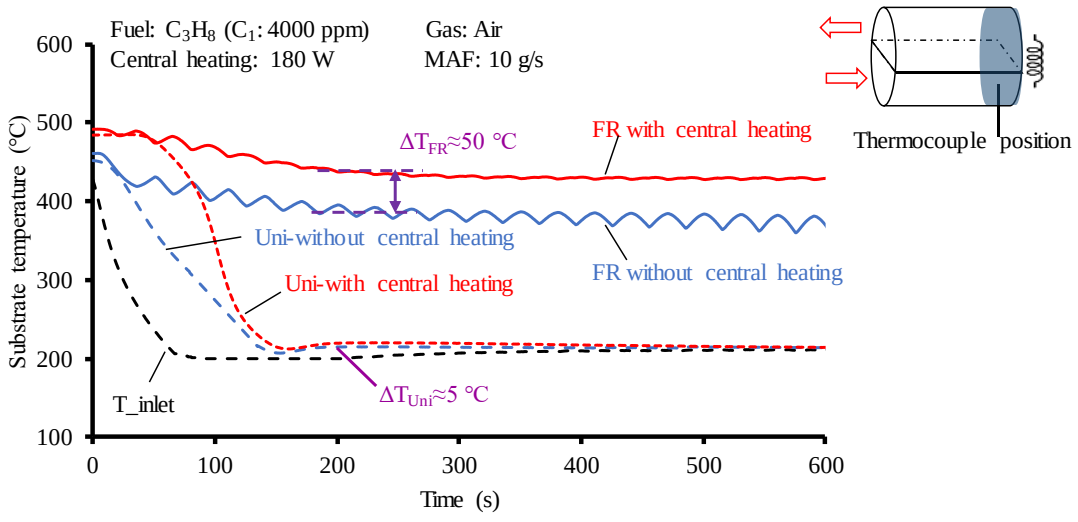

Figure 4.10 Substrate temperature during cooling down process with and without central heating

4.2.2 Substrate Temperature Distribution during Cooling-down Process

To further study the temperature profile of the catalyst under both flow patterns, the temperature distributions along the substrate at four different instances of time during the cooling down process are plotted in Figure 4.11 and Figure 4.12. These instances were taken at 30, 60, 200, and 400 seconds after the beginning of the cooling down process. The mass flow rate for both flow patterns was 10 g/s. The gas temperature was switched to 200 ℃ once the cooling down process started. 4000 ppm C_1 (hydrocarbon) was dosed into the gas at the inlet of the flow bench.

At the initial stage of the cooling down process, for example within 30 seconds, the temperature profiles of the substrate under both unidirectional flow and reversal flow were very similar: 300 ℃ at the front of the substrate, and maximum 470 ℃ in the middle of the substrate. As the substrate was further cooled down by the gas flow, the temperature at the front of the substrate under the unidirectional flow gradually dropped. The high temperature region (over 300 ℃) moved from the middle of the substrates towards the end. The temperatures at the front and in the middle of the substrate dropped to 200 ℃ within 200 seconds after the cooling down started. However, the substrate temperature in the rear was still around 300 ℃ at that moment, as shown in Figure 4.11.

In contrast, the temperature at the corresponding points under reversal flow can be maintained for a much longer time. At 200 seconds after cooling down started, the temperatures in the middle of the substrate remained above 400 ℃. Only the temperatures at the two extremities of the substrate dropped below 300 ℃, as observed from Figure 4.12. The benefits of the flow reversal in heat retention became even more evident after 400 seconds of cooling down. After 400 seconds, the substrate under unidirectional flow

was completely cooled down to 200 ℃ by the flowing gas. However, the temperature in the middle of the substrate under flow reversal pattern still stayed above 400 ℃. This was primarily because the relatively cold flow lowered the substrate temperature at both the front and back segments of the catalyst as the flow direction was periodically reversed. As the flow approached to the middle of the substrate, the temperature difference between the flow and the substrate was reduced because of the heat transfer from the front and back end of the catalyst. Consequently, the heat loss to the flow was minimized and the heat was mostly "trapped" in the middle of the substrate. Therefore, the high temperature region under reversal flow remained in the center of the substrate for 400 seconds. This indicates that the flow reversal system has a better heat trap effect over the unidirectional flow during the substrate cooling down process. This conforms with the previous observations [37, 38].

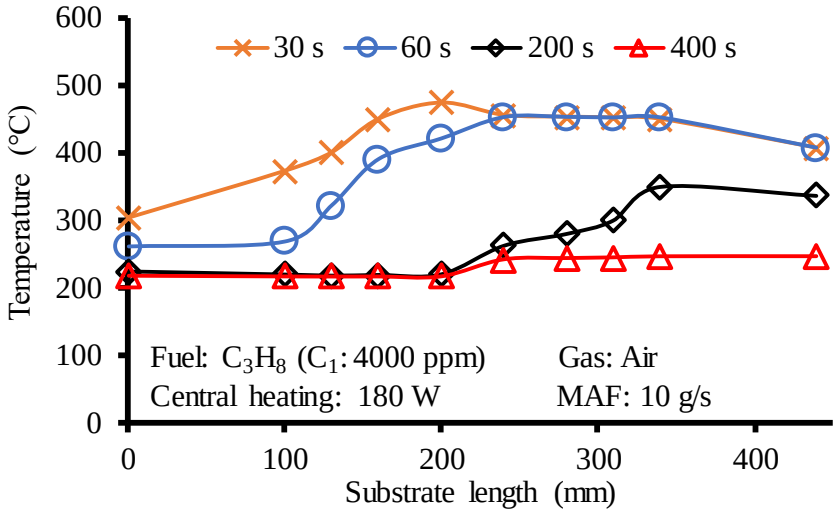

Figure 4.11 Substrate temperature distribution under unidirectional flow

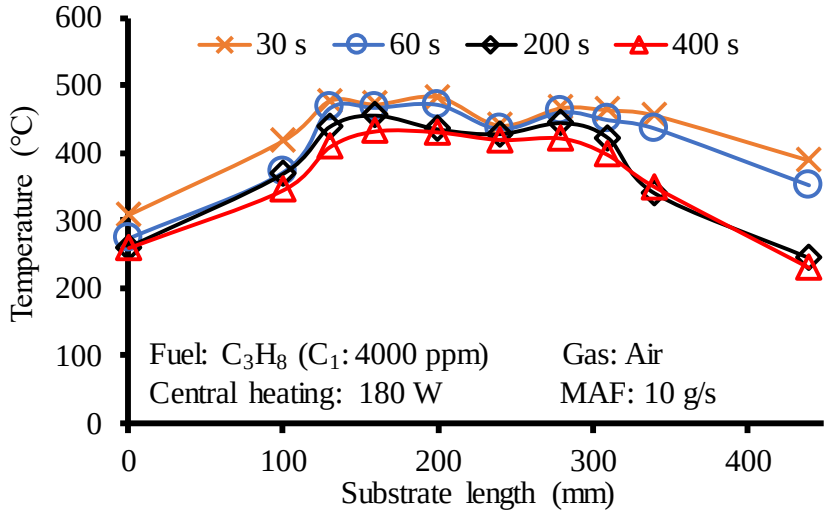

Figure 4.12 Substrate temperature distribution under reversal flow

Additionally, the hydrocarbon conversion efficiency is strongly connected to the catalyst temperature. The hydrocarbon conversion efficiency under unidirectional flow and reversal flow is compared and presented in Figure 4.13. The conversion efficiency under unidirectional flow dropped to less than 50% after 220 seconds. In contrast, owing to the heat retention ability of the flow reversal strategy, the hydrocarbon conversion efficiency under reversal flow was kept around 70% during the same test period.

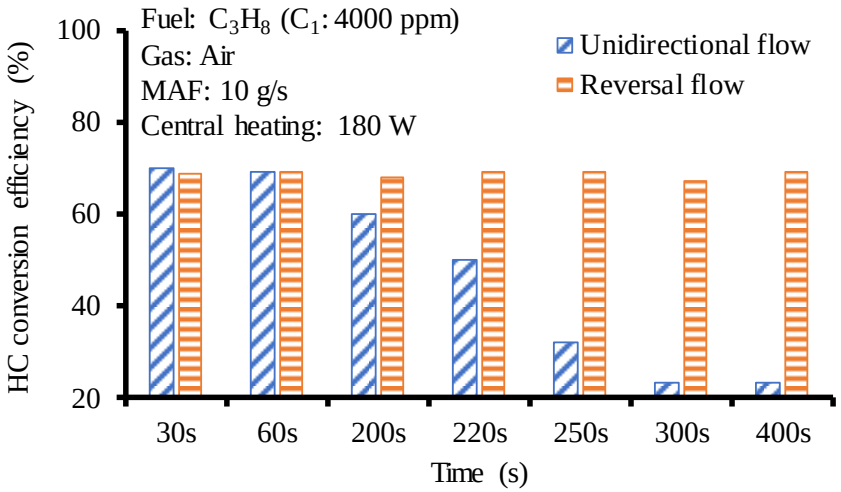

Figure 4.13 HC conversion efficiency of unidirectional flow and reversal flow during cooling down process

CHAPTER 5 CONCLUSIONS AND FUTURE WORK

5.1 Summary of Thesis

A flow reversal research platform was established, and the installation of the platform was documented in detail. The appropriate operational parameters of the flow reversal system were identified under constant inlet gas temperature conditions. The heat retention capabilities of both unidirectional flow and flow reversal strategy were studied during a catalyst cooling down process. The impact of the heat retention of the flow reversal strategy on the HC conversion efficiency of the DOC catalyst was discussed. The major findings of this study are summarized in the following:

1. The flow reversal strategy has a better heat retention capability than the unidirectional flow during the catalyst cooling down process. Periodically reversing the flow direction can maintain the high temperature region at the center of the catalyst for a longer time.

2. During the cooling down process of the catalyst, the HC conversion efficiency of the DOC catalyst with the flow reversal strategy can be maintained at a constantly high level, owing to the better heat retention capability of the flow reversal strategy.

5.2 Future Work

The flow reversal strategy shows a better heat retention capability over the unidirectional flow during the cooling down process of the catalyst, which is beneficial for the improvement of the HC conversion efficiency of the DOC catalyst. The next step of this study is to expand the application of the flow reversal strategy to other aftertreatment catalysts, including LNT, DPF, and a combination of LNT and DOC catalysts.

Further study will focus on the impacts of different operational parameters on the heat retention capability of the flow reversal strategy. Detailed species analysis can be done

through Fourier Transform Infrared Spectroscopy (FTIR) analyzer. Hydrogen generation during DOC oxidation with flow reversal strategy is also a potential area in extending the application scope of the reversal flow.

REFERENCES/BIBLIOGRAPHY

[1] BP, "Statistical Review of World Energy 2018," [Online]. Available: https://www.bp.com/en/global/corporate/energy-economics/statistical-review-of-world energy.html.

[2] IEA, "Electric Vehicles - Fuels & Technologies," [Online]. Available: https://www.iea.org/fuels-and-technologies/electric-vehicles.

[3] X. Yu, N. S. Sandhu, Z. Yang, and M. Zheng, "Suitability of Energy Sources for Automotive Application – A Review," Appl. Energy, vol. 271, 1 August 2020, 115169.

[4] OMEV, "Analysis of Advanced Battery-electric Long haul trucks," [Online]. Available: https://omev.se/2019/09/26/analysis-of-advanced-battery-electric-long-haul-trucks/.

[5] Bureau of Transportation Statistics , "Figure 1 Composition of Diesel and Non-Diesel Fleet: 2014," [Online]. Available: https://www.bts.gov/archive/publications/bts_act_sheets/oct_2015/figure_01.

[6] R. D. Reitz, H, Ogawa, R. Payri, T. Fansler, S. Kokjohn, et al., "IJER editorial: The Future of The Internal Combustion Engine," International Journal of Engine Research, 21(1), 3–10.

[7] J. B. Heywood, "Engine Types and Their Operation," in Internal Combustion Engine Fundamentals, McGraw-Hill College, 1988, Pages 1–37.

[8] Q. Xin and C. F. Pinzon, "Improving The Environmental Performance of Heavy-duty Vehicles and Engines: Key issues And System Design Approaches, " in Alternative Fuels and Advanced Vehicle Technologies for Improved Environmental Performance, 2014, Pages 225-278.

[9] X. Han, "Study of Fuels and Fuelling Strategies for Enabling Clean Combustion in Compression Ignition Engines," PhD Theses, University of Windsor, Canada, 2014.

[10] T. V Johnson, "Review of Vehicular Emissions Trends," SAE Technical Paper, 2015-01-0993, 2015.

[11] W. Siebenpfeiff, "On- und Off -Highway- Motoren, " ISSN 2198-7432, published in 2016.

[12] M. Brandt, A. Hettinger, A. Schneider, H. Senftleben, and T. Skowronek, “Extension of Operating Window for Modern Combustion Systems by High Performance Ignition,” 3rd International Conference, November 3–4, 2016, Berlin, Germany.

[13] Toyota, “2.0-liter Dynamic Force Engine, a New 2.0-liter Direct-injection, Inline 4-cylinder Gasoline Engine,” [Online]. Available: https://global.toyota/en/mobility/tnga/powertrain 2018/engine/.

[14] H. Wei, T. Zhu, G. Shu, L. Tan, and Y. Wang, “Gasoline Engine Exhaust Gas Recirculation - A review,” Appl. Energy 99 (2012) 534–544.

[15] M. Jeftic, “Enhanced Aftertreatment Performance : Post Injection Characterization and Long Breathing with Low NOx Combustion,” PhD thesis, University of Windsor, 2016.

[16] U. Asad, “Advanced Diagnostics, Control and Testing of Diesel Low Temperature Combustion, ” PhD thesis, Univeristy of Windsor, 2009.

[17] C. A. Idicheria and L. M. Pickett, “Soot Formation in Diesel Combustion under High-EGR Conditions,” SAE Technical Paper 2015-01-3834, 2005.

[18] S. Kohketsu, K. Mori, K. Sakai, and T. Hakozaki, “EGR Technologies for A Turbocharged And Intercooled Heavy-duty Diesel Engine,” SAE Technical Paper, 970340, 1997.

[19] U. Asad and M. Zheng, “EGR oxidation and Catalytic Fuel Reforming for Diesel Engines,” ASME 2008 Internal Combustion Engine Division Spring Technical Conference, ICES2008-1684, 2008.

[20] A. K. Agarwal, A. P. Singh, and R. K. Maurya, “Evolution, Challenges and Path Forward for Low Temperature Combustion Engines,” Progress in Energy and Combustion Science, vol. 61, July 2017, Pages 1–56.

[21] Z. Chen, J. Liu, Z. Wu, and C. Lee, “Effects of Port Fuel Injection (PFI) of N-butanol And EGR on Combustion And Emissions of A Direct Injection Diesel Engine,” Energy Convers. Manag., vol. 76, pp. 725–731, Dec. 2013.

[22] R. K. Maurya and A. K. Agarwal, “Experimental Study of Combustion and Emission Characteristics of Ethanol Fuelled Port Injected Homogeneous Charge Compression Ignition (HCCI) Combustion Engine,” Appl. Energy, Volume 88, Issue 4, April 2011, Pages 1169-1180.

[23] A. S. Ayodhya and K. G. Narayanappa, “An Overview of Aftertreatment Systems for Diesel Engines,” Environmental Science and Pollution Research 25(1–4), October 2018.

[24] M. M. Azis, X. Auvray, L. Olsson, D. Creaser, “Evaluation of H2 Effect on NO Oxidation over a Diesel Oxidation Catalyst,” Appl Catal B Env., vol. 179, pp. 542–550, 2015.

[25] Z. Huang, X. Qiao, W. Zhang, J. Wu, and J. Zhang, “Dimethyl Ether as Alternative Fuel for CI Engine and Vehicle,” Front. Energy Power Eng. China, vol. 3, no. 1, pp. 99–108, Mar. 2009.

[26] M. Zheng and S. Banerjee, “Diesel Oxidation Catalyst and Particulate Filter Modeling in Active - Flow Configurations,” Appl. Therm. Eng., vol. 29, no. 14–15, pp. 3021–3035, Oct. 2009.

[27] A.Russell and W.S.Epling, “Diesel Oxidation Catalyst, " Catalysis Review: Sci. Eng., vol. 53, no. 4, pp. 337–423, 2011.

[28] M. Zheng, G. T. Reader, and M. Wang, “Investigation of Active Flow Control on Diesel Engine Aftertreatment,” J. Propuls. Power, vol. 24, no. 2, pp. 376–383, Mar. 2008.

[29] M. Zheng and G. T. Reader, “Energy Efficiency Analyses of Active Flow Aftertreatment Systems for Lean Burn Internal Combustion Engines,” Energy Convers. Manag., vol. 45, no. 15–16, pp. 2473–2493, 2004.

[30] M. Zheng, E. Mirosh, W. Klopp, D. Ulan, M. Pardell, P. Newman, et al., “Development of a Compact Reverse-flow catalytic converter for diesel dual fuel LEV,” SAE Technical Paper, 1999-01-3558, 1999.

[31] G. T. Reader, S. Banerjee, M. Wang, and M. Zheng, “Energy Efficiency Analysis of Active-flow Operations in Diesel Engine Aftertreatment,” SAE Technical Paper, 2006-01-3286, 2006.

[32] C. Schenk, C. Laroo, B. Olson, and L. Fisher, “Four-flow Path High-efficiency NOX and PM Exhaust Emission Control System for Heavy-duty on-highway Diesel Engines,” SAE Technical Paper, 2003-01-2305, 2003.

[33] A. G. Konstandopoulos and M. Kostoglou, “Reciprocating Flow Regeneration of Soot Filters,” Combust. Flame, vol. 121, no. 3, pp. 488–500, 2000.

[34] A. Algieri, M. Amelio, and P. Morrone, “A Comparative Energetic Analysis of Active and Passive Emission Control Systems Adopting Standard Emission Test Cycles,” Model. Simul. Eng., vol. 2012, 2012.

[35] Y. S. H. Matros and G. A. Bunimovich, “Reverse-flow Operation in Fixed Bed Catalytic Reactors,” Catal. Rev. - Sci. Eng., vol. 38, no. 1, pp. 1–68, 1996.

[36] B. Liu, R. E. Hayes, M. D. Checkel, M. Zheng, and E. Mirosh, “Reversing Flow Catalytic Converter for a Natural Gas/Diesel Dual Fuel Engine,” Chem. Eng. Sci., vol. 56, no. 8, pp. 2641–2658, 2001.

[37] M. Zheng, E. A. Mirosh, and G. T. Reader, “Improved Reversing Flow Catalytic Converter for Internal Combustion Engines, ” Canada patent, CA2508159A1, 2006/11/24.

[38] M. Zheng, D. Wang, G. T. Reader, and M. Wang, “Empirical and Theoretical Investigations of Active-flow Control on Diesel Engine Aftertreatment,” SAE Technical Paper, 2006-01-0465, 2006.

[39] D.K. Irick, K. Nguyen, “Energy Efficient Thermal Management for Natural Gas Engine Aftertreatment via Active Flow Control," OSTI Annual Technical Progress Report, April 2004. The University of Tennessee.

[40] V. O. Strots, G. A. Bunimovich, Y. S. Matros, M. Zheng, and E. A. Mirosh, “Novel Catalytic Converter for Natural Gas Powered Diesel Engines,” SAE Technical Paper, 980194, 1998.

[41] K. Hanamura, R. Echigo, and S. A. Zhdanok, “Superadiabatic Combustion in a Porous Medium,” Int. J. Heat Mass Transf., vol. 36, no. 13, pp. 3201–3209, 1993.

[42] S. S. Smith, “Reverse-Flow Oxidation Catalyst with Supplemental Fuel Injection for Lean-Burn Natural Gas Engines,” Master degree Thesis, The University of Tennessee, 2005.

[43] C. McAtee, G. McCullough,R. Douglas, and L. Glover, “The Effect of De-Greening and Pre-Treatment on Automotive Catalyst Performance, ” SAE Technical Paper 2011-24-0188, 2011.

[44] M. Zheng, G.T. Reader, D. Wang, J. Zuo, M. Wang, et al., “A Thermal Analysis of Active-Flow Control on Diesel Engine Aftertreatment,” SAE Technical Paper, 2004-01-3020, 2004.

[45] C. Aversa, S. Yu, M. Jeftić, G. Bryden, and M. Zheng, “Long Breathing Lean NOx Trap Regeneration with Supplemental N-butanol,” Proceedings of the Institution of Mechanical Engineers, Part D: Journal of Automobile Engineering, 233(3), 661–670.

[46] D. Purohit, S. Dev, Q. Tan, N. Sandhu, et al., “An Investigation on the Regeneration of Lean NOX Trap Using Ethanol and N-butanol,” SAE Technical Paper, 2019-01-0737, 2019.

[47] L. Liang, H. Zhu, N. S. Sandhu, D. Purohit, and X. Yu, “An Investigation on the Regeneration of Lean NOX Trap Using Dimethyl Ether,” SAE Technical Paper, 2020-01-1354, 2020.

[48] S. Erkfeldt, A. Palmqvist, and E. Jobson, “NOX Reduction Performance of Lean NOX Catalyst and Lean NOX Adsorber Using DME as Reducing Agent,” Top. Catal., vol. 42–43, no. 1–4, pp. 149–152, 2007.

[49] M. Jeftić and M. Zheng, “Lean NOx Trap Supplemental Energy Savings with A Long Breathing Strategy,” Proc. Inst. Mech. Eng. Part D J. Automob. Eng., vol. 227, no. 3, pp. 400–408, 2013.

APPENDIX A: LEAN NO_X TRAP REGENERATION USING DIMETHYL ETHER

The findings summarized in this appendix have been published in SAE technical paper 2020-01-1354.

Dimethyl ether (DME) is regarded as one type of alternative fuels in automotive. It has a similar cetane number (#55-60) as diesel (#55), and a number of advantages over the conventional fossil fuels, such as low CO and NO_X emissions, nearly no soot and sulfur. Therefore, DME is proposed to suppress NO_X - soot trade-off in CI engines. In this appendix, the possibility of using DME as a reductant for LNT regeneration is discussed. A comparison between DME and other different reductants, including n-butanol, ethanol, and diesel, is summarized in this appendix [15, 45, 46, 47, 48, 49].

Experimental Setup and Methodology

Experiment of using dimethyl ether (DME) as a reductant for LNT regeneration is performed on the aftertreatment flow bench. The experiment setup is shown in Figure A- 1. The test conditions and parameters are summarized in Table A-1.

As DME is in gaseous phase under ambient condition, the injection quantity of the compressed DME (5 bar) is calibrated offline by weighting method. During the calibration, stainless steel gas bottle with DME under 5 bar is placed on the top of the scale (resolution of 0.001 g) to get the instant weight of the gas bottle. FPGA controller is used to vary the injection duty cycles and frequencies to achieve various injection quantities. For each calibrated injection quantity, one thousand times of injection are conducted, and the weight

change is read from the scale and recorded. The injection quantity of each shot is calculated through the recorded weight change of the gas bottle.

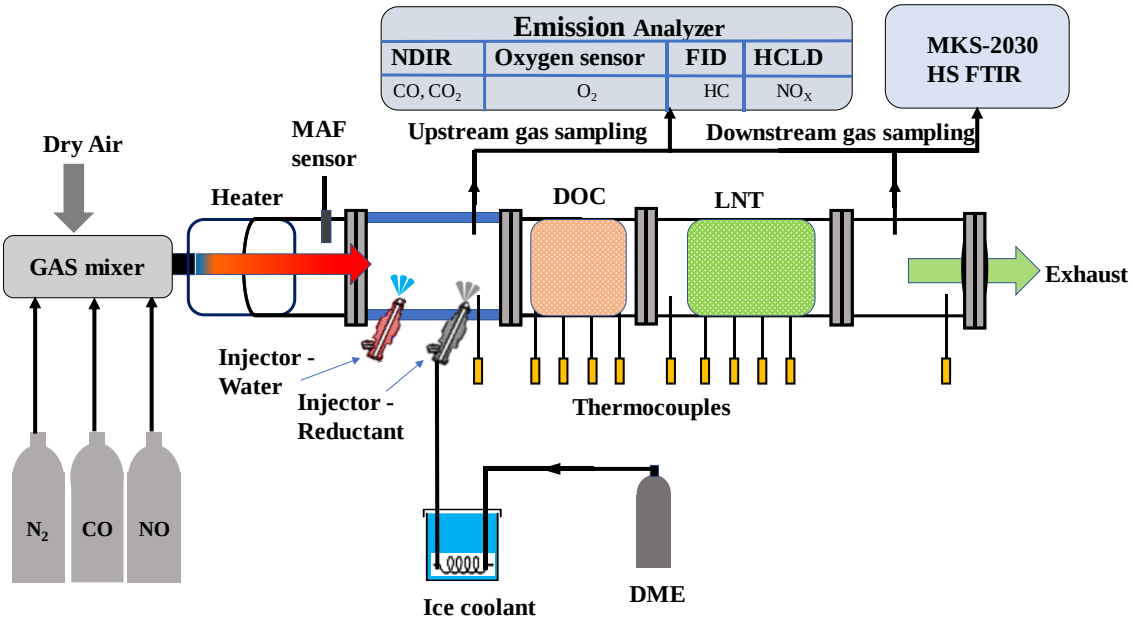

Figure A- 1 Schematic of LNT regeneration experimental setup

In this study, CAI-600S heated chemiluminescence detector (HCLD) and Fourier-transform infrared spectroscopy (FTIR) analyzer (MKS2030-DS) are both used to continuously measure the NO_X concentration, and other by-products generated during the LNT regeneration process. The LNT catalyst is heated to 350 ℃ before the test, as the conversion of DME is reported to nearly complete at 300 ℃ and above.

Table A-1 Test parameters of using DME for LNT regeneration

LNT temperature (℃)	350	O_2 concentration (%)	3
NO_X-feed-in gas (ppm)	200	H_2O concentration (%)	6
Stored NO_X in LNT (g)	0.2	Catalyst volume (L)	0.2
Space velocity (h^{-1})	80,000	DME injection quantity (g)	0.45, 0.6, 0.8, 1.4, 1.7, 2.5, 2.7, 3.2

The LNT regeneration process starts with the NO_X adsorption. During the NO_X adsorption period, 200 ppm NO_X is continuously fed into the LNT catalyst until the accumulated NO_X on the catalyst reaches to 0.2 g. The absorbed NO_X quantity is calculated according to Equation A-1.

$$NOx_{stored\ quantity} = (NOx_{Inlet} - NOx_{outlet}) \times Mass\ flow\ rate \quad \text{(A-1)}$$

The NO_X trapping efficiency (as shown in Equation A-2) is verified before regeneration starts. Relevant results have shown that the NO_X trapping efficiency of the tested LNT catalyst can be maintained at 98% during the adsorption period.

$$NOx_{trapping\ efficiency} = \frac{mNOx_{intake} - mNOx_{slip\ during\ adsorption}}{mNOx_{intake}} \quad \text{(A-2)}$$

After the NO_X adsorption process, reductant and water are injected into the flow bench to start the regeneration process once the LNT temperature is stabilized. During regeneration, the absorbed NO_X on the LNT catalyst is mainly converted to N_2, and partially converted to NH_3, and N_2O. In order to control the boundary condition of the experiment, pure N_2 and 5% CO gas are used to remove any remaining NO_X on the catalyst after each regeneration cycle. At the end of each test cycle, the catalyst is also flushed with THC-free air. The regeneration efficiency is calculated according to Equation A-3.

$$Regeneration\ efficiency\ = \frac{NOx_{stored} - NOx_{slip\ during\ purge}}{NOx_{stored}} \quad \text{(A-3)}$$

Results and Discussion

In order to study the potential of using DME as a reductant for LNT regeneration, DME with different quantities (from 0.45 g to 3.2 g) is injected to the flow bench to start the regeneration process. The slipped NO_X when injecting 0.45 g DME is shown in

Figure A- 2. As can be seen, very little NO_X is slipped out during both regeneration and purging processes under this DME injection quantity.

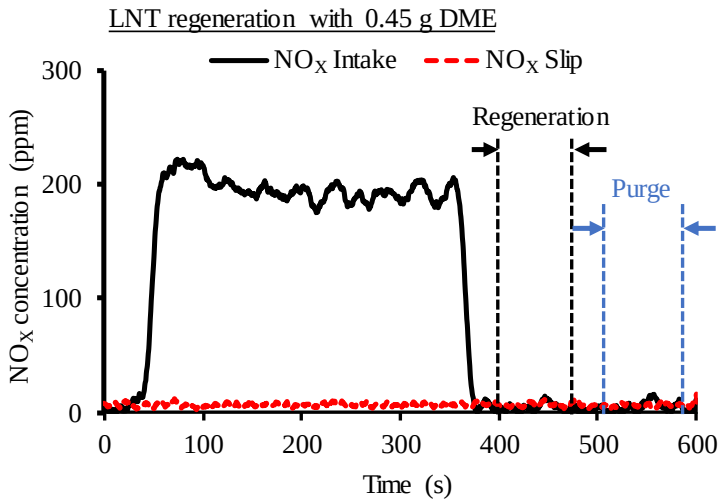

Figure A- 2 LNT regeneration under 0.45 g DME injection quantity

More NO_X is slipped out when injecting more DME for regeneration. However, the slipped NO_X starts to reduce once the DME injection quantity is beyond 1.7 g. The slipped NO_X and the formed CH_4 under different DME injection quantities are shown in Figure A- 3.

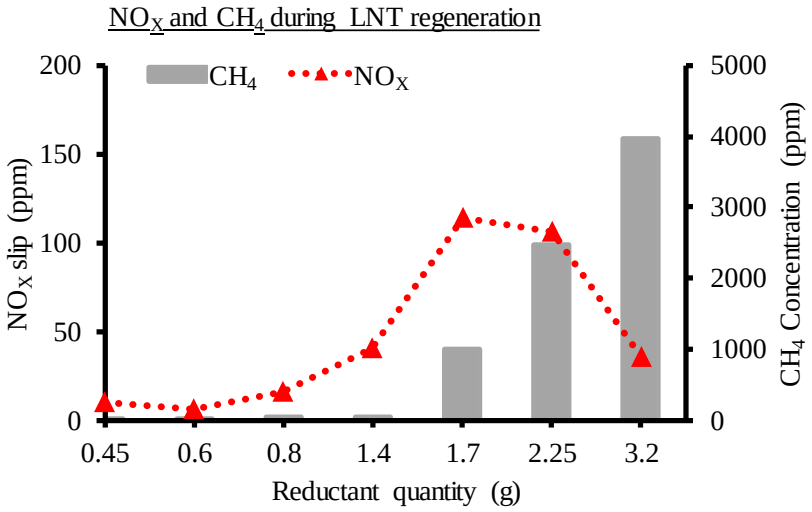

Figure A- 3 NO_X slip and reformed CH_4 under different injection quantity

The slipped DME and reformed CH_4 under different DME injection quantities are illustrated in Figure A- 4. Less DME is slipped out while more CH_4 is formed when rising

the DME injection quantity from 0.8 g to 3.2 g. The increasing trend of CH_4 can be partially explained by the DME decompensation in which DME decompensates into H_2 and CH_4.

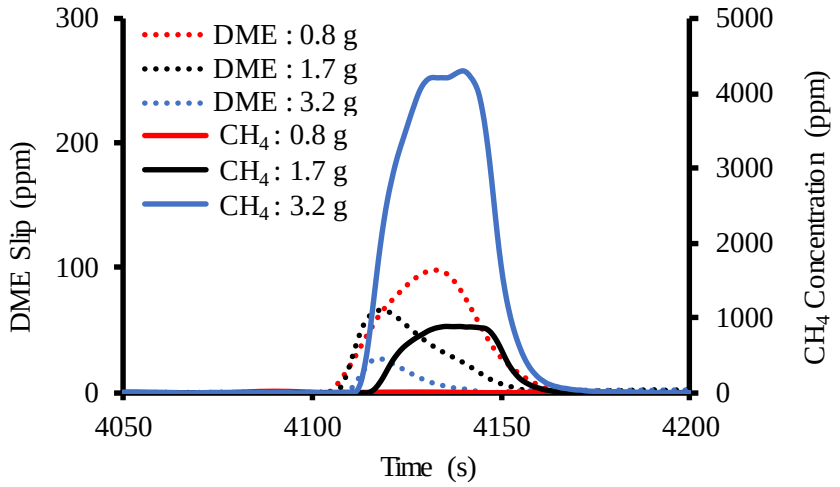

Figure A- 4 Slipped DME and reformed CH_4 under different injection quantity

In order to evaluate the performance of DME as the reductant of LNT regeneration, the slipped NO_X and other by-products of using DME as a reductant are compared with different reductants, including n-butanol, diesel, ethanol. The peak slipped NO_X for these four types of reductants under different injection quantities is shown in Figure A- 5. The peak quantity of the formed N_2O under the same condition is illustrated in Figure A- 6. The least NO_X is slipped out when using DME as the reductant for LNT regeneration, as compared to other tested reductants. This indicates that DME has a higher conversion efficiency. The lowest N_2O is formed when using DME as the reductant. As N_2O is one of the green house gases, this indicates another benefit of using DME for LNT regeneration.

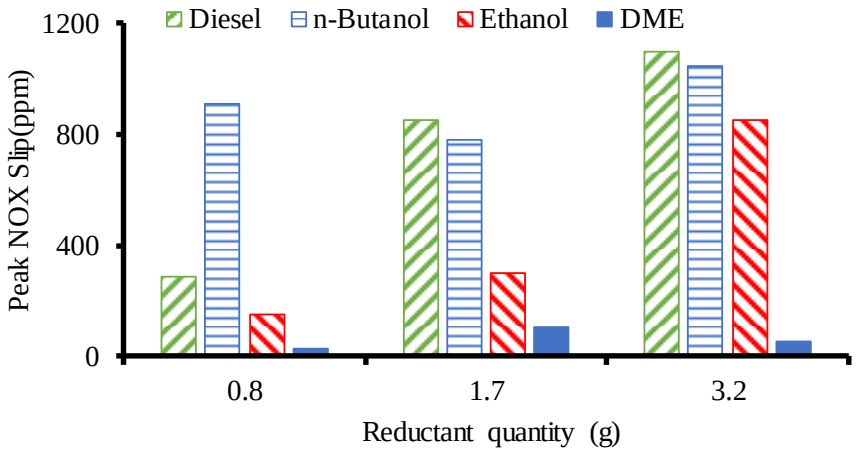

Figure A- 5 Peak NO_X slip with different reductants

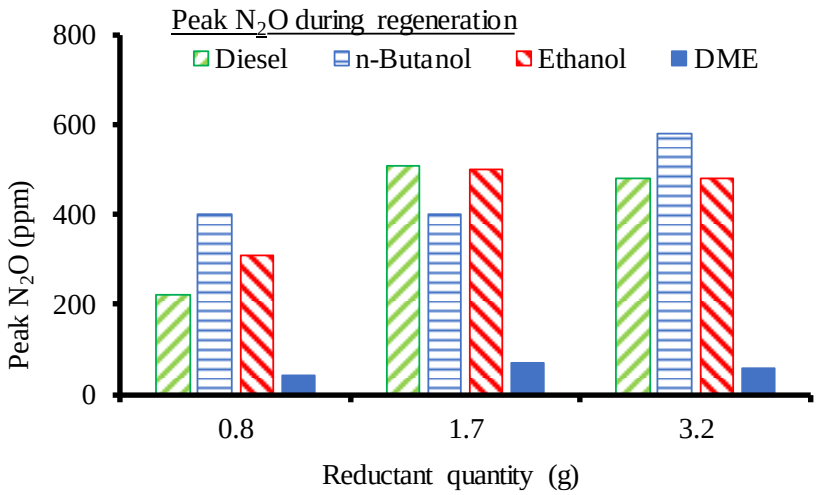

Figure A- 6 Peak N_2O during regeneration with different reductants

The peak NH_3 generated during the LNT regeneration when using these four types of reductants is shown in Figure A- 7. More NH_3 is formed when using ethanol and n-butanol as reductants, as compare to Diesel and DME. This is mainly because more H_2 is generated using n-butanol and ethanol during regeneration, leading to a higher formation of NH_3.

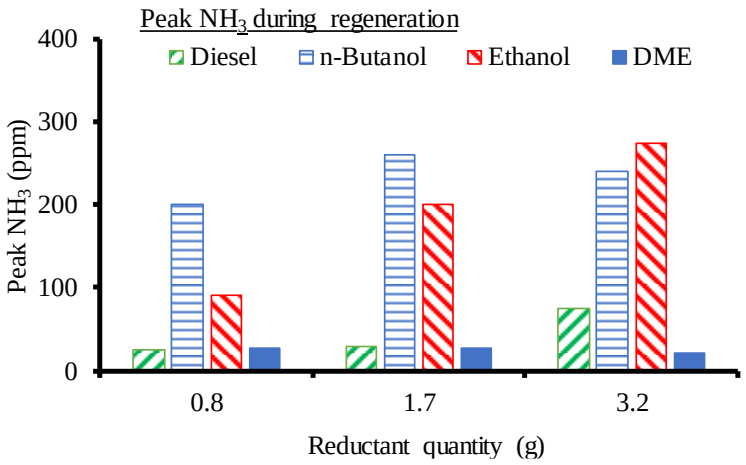

Figure A- 7 Peak NH_3 during regeneration with different reductants

The last by-product discussed here is methane (CH_4), as it is also a greenhouse gas. The peak value of CH_4 production with different reductants is shown in Figure A- 8. A general increasing trend of CH_4 production can be seen when increasing the injection quantity of the reductants. Among these four types of reductants, ethanol has the highest CH_4 production. DME has a moderate CH_4 production, as compared to that of diesel and n-butanol. For example, when injecting 3.2 g of reductants, the peak value of CH_4 is up to 41859 ppm for ethanol, and 3955 ppm for DME, while only 71 ppm for diesel and 340 ppm for n-butanol.

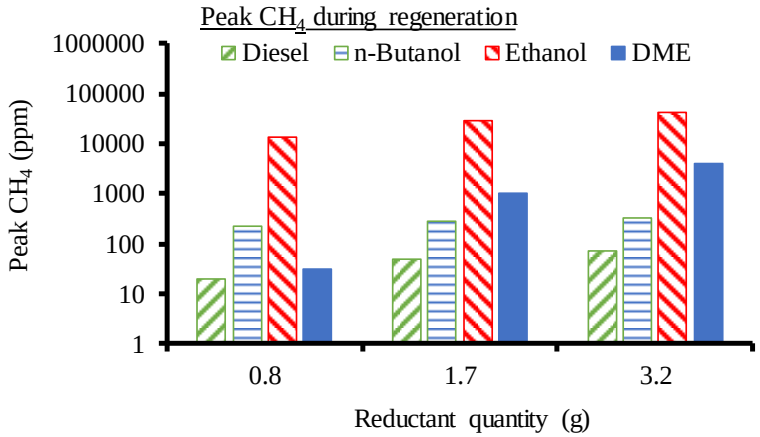

Figure A- 8 Peak CH_4 during regeneration with different reductants

Conclusions

During the LNT regeneration process, DME has shown a higher regeneration efficiency and lower productions of N_2O and NH_3 than other investigated reductants. However, a higher amount of CH_4 is formed when the same amount of DME is injected for LNT regeneration, as compared to diesel injection. This might be one drawback of using DME as the reductant of LNT regeneration, as CH_4 is one type of greenhouse gases.

APPENDIX B: RAPID COMPRESSION MACHINE PLATFORM PREPARATION

Setting up a rapid compression machine (RCM) platform is one of the projects that author has been working on. A RCM can simulate the compression and ignition process under an engine-like condition, as the high pressure and high temperature generated during the rapid compression process of RCM is close to the real engine process. Therefore, RCM can be used to study the spark ignition and the chemical kinetics under high pressure and temperature condition.

The current RCM design consists of a pneumatic driving, a hydraulic cylinder serving as an actuator and brake, and a compression cylinder. The preparation of the RCM is initiated by the previous researchers in author's lab. The author is mainly responsible for improving the design, machining and installing the components. This project has also received a lot of help from Ford company and the machine shop in the University of Windsor's. This appendix is a detailed documentation for the current RCM design.

The compression cylinder in the current RCM is designed with a stroke of 230 mm and a bore size of 50 mm. The maximum designed compression ratio is 21. The schematic of the assembly is shown in Figure B- 1. Each main part of the RCM is explained and documented in the following sections of this appendix.

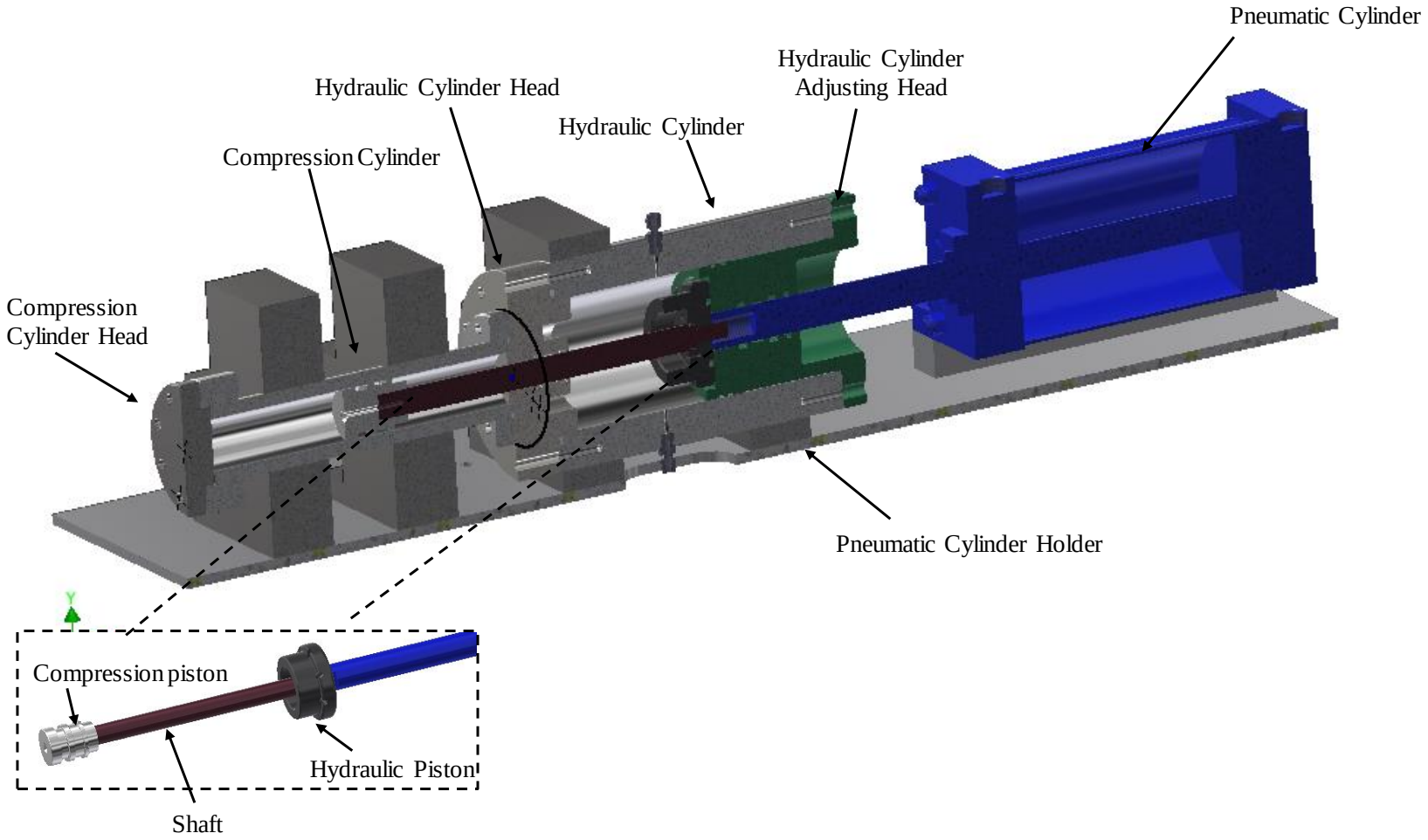

Figure B- 1 Schematic of RCM assembly

B1.1 Pneumatic Section

The pneumatic cylinder is purchased from Peninsular Cylinder Company with customized parameters. The picture of the pneumatic cylinder is shown in Figure B- 2. The bore size of the pneumatic cylinder is 6". The maximum pressure that the cylinder can standard is 250 psi (17 bar). There are two 3/4" ports in the cylinder for air inlet and outlet. A pressure gauge is installed on the cylinder to monitor the inlet pressure.

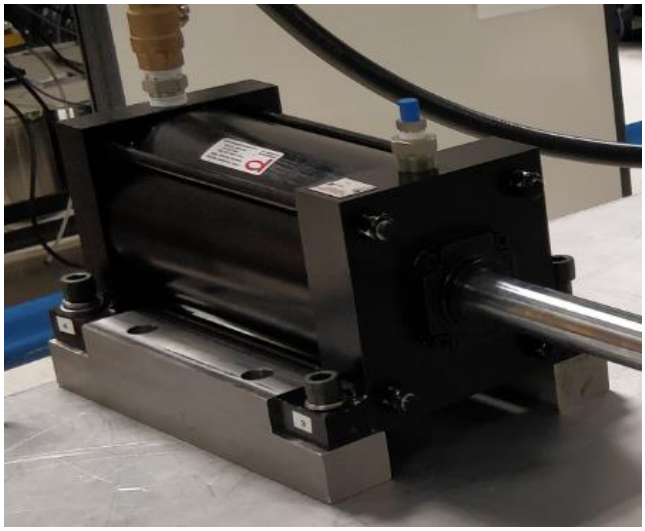

Figure B- 2 Pneumatic cylinder

B1.2 Hydraulic Section

The hydraulic system mainly includes a hydraulic cylinder, an adjusting head, a hydraulic piston, a cylinder cap, and a hydraulic oil pump. The hydraulic cylinder, adjusting head, and the cylinder cap are all made of stainless steel.

B1.2.1 Hydraulic Cylinder Adjusting Head

The hydraulic cylinder adjusting head is shown in Figure B- 3. It is designed to connect to the hydraulic cylinder through ten M10 bolts.

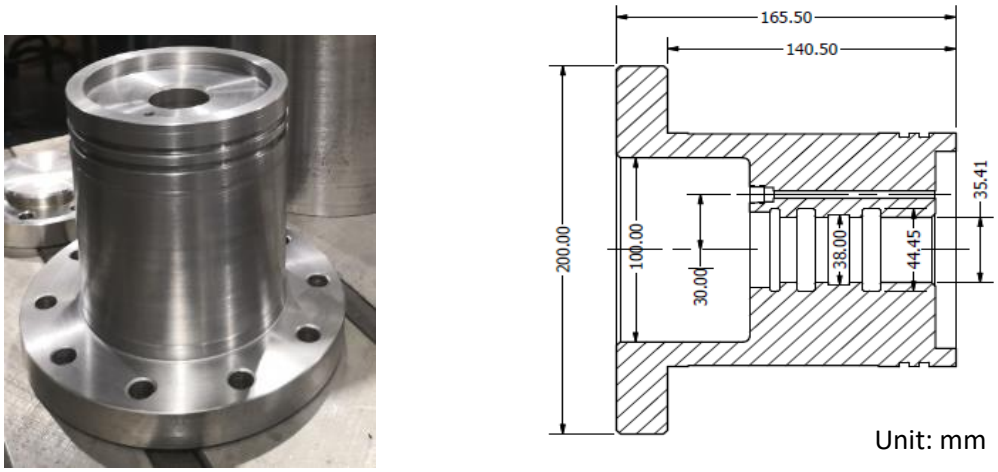

Figure B- 3 Hydraulic adjusting head

The overall compression ratio of the compression cylinder can be changed by increasing or reducing the adjusting ring between the hydraulic cylinder and the adjusting head, as shown in Figure B- 4.

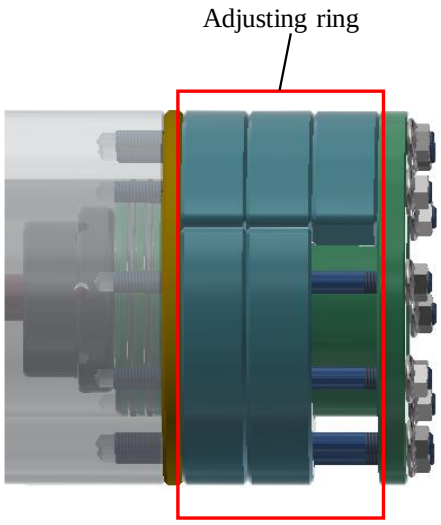

Figure B- 4 Hydraulic adjusting rings

B1.2.2 Hydraulic Cylinder

The hydraulic cylinder in the current RCM design is 294.5 mm long. The inner diameter of the cylinder is 127 mm, as shown in Figure B- 5. There are two through holes drilled on the cylinder wall: the one on the top is used to release air during oil feed-in, and the other one at the bottom is used for hydraulic oil feed-in and release.

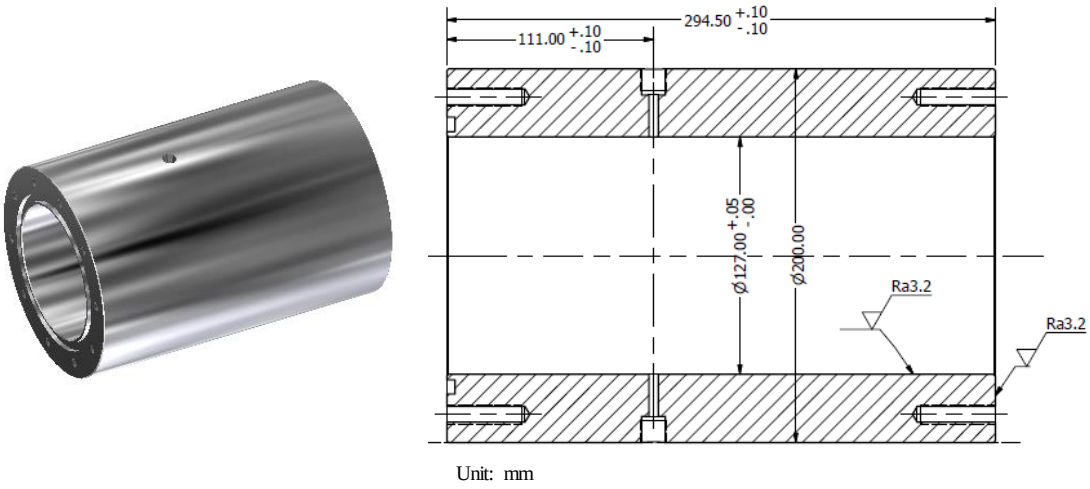

Figure B- 5 Hydraulic cylinder

B1.2.3 Hydraulic Piston

The hydraulic piston is shown in Figure B- 6. It is designed with several functions in the RCM system. Firstly, the hydraulic piston holds the compression piston before the compression process starts. At this position, the rear of the hydraulic piston is against to the hydraulic adjusting head and the front surface of the piston is pressurized by the oil. The secondary function of the hydraulic piston is serving as a stopper to stop the compression piston at the end of compression. At that point, the front of the hydraulic position enters the designed groove, and the pressure generated from the feed-in oil decelerates the piston. Moreover, the hydraulic system can also control the compression speed by controlling the hydraulic oil releasing rate through the venting hole.

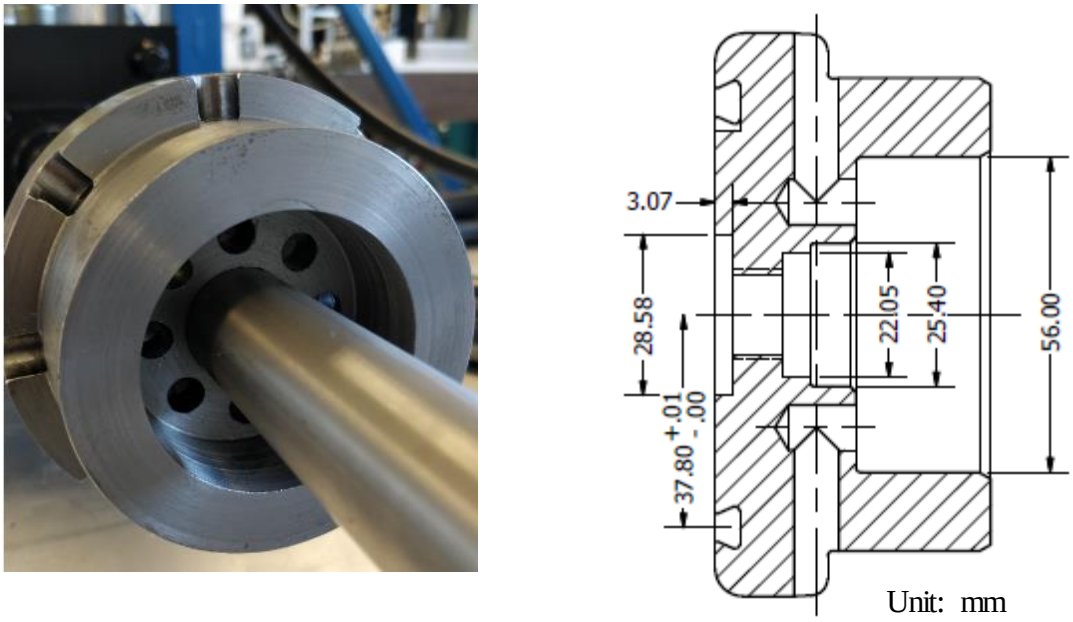

Figure B- 6 Hydraulic piston

B1.3 Compression Section

The compression system in the RCM design includes a compression cylinder, a compression piston, and a compression cylinder cap. The compression cylinder and the compression head are all made of stainless steel. The assembly is shown in Figure B- 7.

Figure B- 7 Assembly of compression cylinder

B1.3.1 Compression Cylinder

The detailed compression cylinder dimensions are shown in Figure B- 8. The cylinder has a bore size of 50 mm, and a total length of 322 mm.

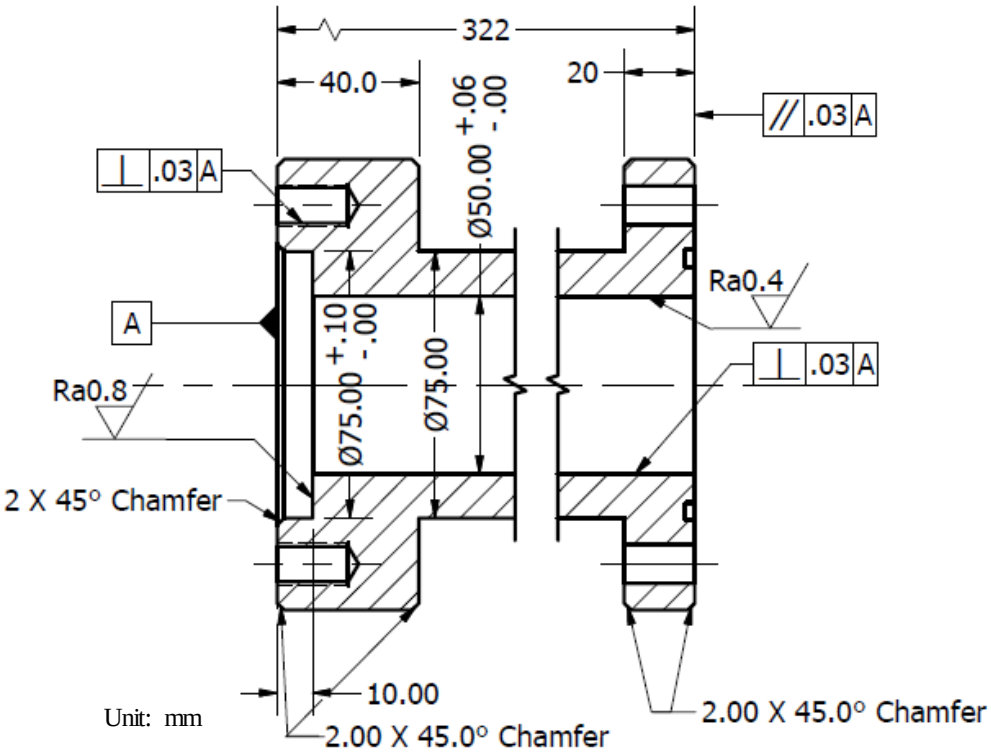

Figure B- 8 Dimension of compression cylinder

B1.3.2 Compression Cylinder Cap

The current compression cylinder cap is made of stainless steel. It is designed with a pressure transducer mounting port and a gas inlet/outlet port, as shown in Figure B- 9. The Swagelok rising valve can be used to control the gas in and out. The compression cylinder cap is fastened to the compression cylinder through ten M10 bolts. A copper gasket with a thickness of 0.55 mm is used for the surface seal, as shown in Figure B- 10. In case of optical diagnosis, this metal cap can be replaced by an optical combustion chamber.

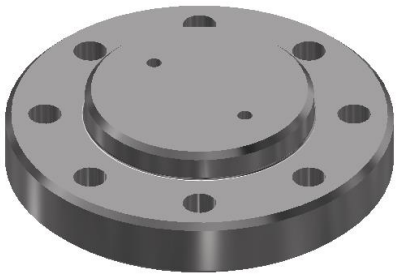

Figure B- 9 Compression cylinder head

Figure B- 10 Gasket for compression chamber

B1.3.3 Compression Piston

The compression piston is in a crevice deign, as shown in Figure B- 11. The piston is designed into two parts in order to easily install the sealing components and the piston rod. The detailed design of the crevice piston is shown in Figure B- 12.

Figure B- 11 Compression piston

The main sealing components used in the current RCM design are listed in Table B-1, including the part number and the function.

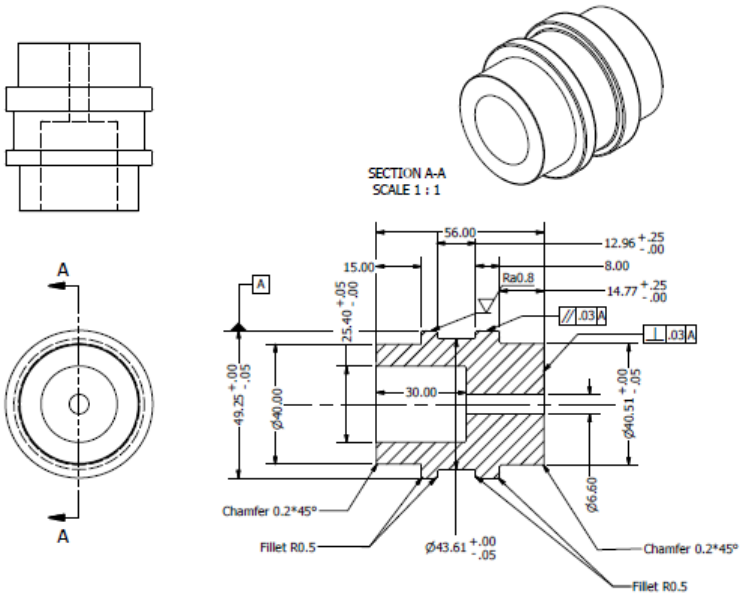

Figure B- 12 Drawing of compression piston

Table B-1 Sealing components list

Part number	Function
W6-01500-0375-bc-sd	Pneumatic rod seal
Ubr-1870-1375-312-tc	Hydraulic seal
Dt-1375	Hydraulic wiper
WM-01125-0500-BC-SD	Compression rod wearing
ZBR-1250-1000-250TC	Compression rod seal

VITA AUCTORIS

NAME:	Li Liang
PLACE OF BIRTH:	Xinjiang, P.R.China
YEAR OF BIRTH:	1981
EDUCATION:	Central South University, Changsha, Hunan, P.R. China 1999-2003 B.Eng. University of Windsor, Windsor, ON, Canada 2018-2020, M.A.Sc